



Article

Meteorological Drought Variability over Africa from Multisource Datasets

Kenny T. C. Lim Kam Sian ^{1,2} , Xiefei Zhi ³, Brian O. Ayugi ^{4,*} , Charles Onyutha ⁵ , Zablon W. Shilenje ⁶ and Victor Ongoma ⁷

¹ School of Atmospheric Science and Remote Sensing, Wuxi University, Wuxi 214105, China; kennylimks@cwxy.edu.cn

² Wuxi Institute of Technology, Nanjing University of Information Science & Technology, Wuxi 214105, China

³ Key Laboratory of Meteorological Disasters, Ministry of Education (KLME)/Collaborative Innovation Center on Forecast and Evaluation of Meteorological Disasters (CIC-FEMD), Nanjing University of Information Science and Technology, Nanjing 210044, China; zhi@nuist.edu.cn

⁴ Department of Civil Engineering, Seoul National University of Science and Technology, Seoul 01811, Republic of Korea

⁵ Department of Civil and Environmental Engineering, Kyambogo University, Kyambogo, Kampala P.O. Box 1, Uganda; conyutha@kyu.ac.ug

⁶ Department of Atmospheric Physics, Faculty of Mathematics, Charles University, V Holešovičkách 2, 180 00 Prague 8, Czech Republic; zshilenje@wmo.int

⁷ International Water Research Institute, Mohammed VI Polytechnic University, Lot 660, Hay Moulay Rachid, Ben Guerir 43150, Morocco; victor.ongoma@um6p.ma

* Correspondence: bayugi@seoultech.ac.kr



Citation: Lim Kam Sian, K.T.C.; Zhi, X.; Ayugi, B.O.; Onyutha, C.; Shilenje, Z.W.; Ongoma, V. Meteorological Drought Variability over Africa from Multisource Datasets. *Atmosphere* **2023**, *14*, 1052. <https://doi.org/10.3390/atmos14061052>

Academic Editor: Ognjen Bonacci

Received: 9 May 2023

Revised: 6 June 2023

Accepted: 14 June 2023

Published: 19 June 2023



Copyright: © 2023 by the authors. Licensee MDPI, Basel, Switzerland. This article is an open access article distributed under the terms and conditions of the Creative Commons Attribution (CC BY) license (<https://creativecommons.org/licenses/by/4.0/>).

Abstract: This study analyses the spatiotemporal variability of meteorological drought over Africa and its nine climate subregions from an ensemble of 19 multisource datasets (gauge-based, satellite-based and reanalysis) over the period 1983–2014. The standardized precipitation index (SPI) is used to represent drought on a 3-month scale. We analyse various drought characteristics (duration, events, frequency, intensity, and severity) for all drought months, and moderate, severe, and extreme drought conditions. The results show that drought occurs across the continent, with the equatorial regions displaying more negative SPI values, especially for moderate and severe droughts. On the other hand, Eastern Sahara and Western Southern Africa portray less negative SPI values. The study also reveals that extreme drought months have the largest interannual variability, followed by all drought months and severe drought months. The trend analysis of SPI shows a significantly increasing trend in drought episodes over most regions of Africa, especially tropical areas. Drought characteristics vary greatly across different regions of Africa, with some areas experiencing longer and more severe droughts than others. The equatorial region has the highest number of drought events, with longer durations for severe and extreme drought months. The Eastern Sahara region has a low number of drought events but with longer durations for moderate, severe, and extreme drought months, leading to an overall higher drought severity over the area. In contrast, Western Southern Africa and Madagascar display a consistently low drought severity for all categories. The study demonstrates the importance of conducting drought analysis for different drought levels instead of using all drought months. Drought management and adaptation strategies need to enhance community resilience to changing drought situations and consider drought variability in order to mitigate different impacts of drought across the continent.

Keywords: climate change; precipitation extremes; drought; gauge-based products; satellite products; reanalysis products; Africa

1. Introduction

Africa is facing an imminent socioeconomic threat due to the increasing intensity and frequency of extreme weather and climate events, which are expected to worsen

with global warming [1]. Studies indicate that all African subregions experienced an increase in temperature in the past 60 years [2]. Many developing countries in Africa rely on rainfed agriculture for food production and as a source of livelihood. Hence, they are vulnerable to the effects of climate change [3]. Parts of the continent, such as Southern Africa, have observed and projected an increase in aridity and agricultural and ecological droughts [1,4]. According to Kedir [5], an increase in drought will slow the realisation of sustainable development goals and threaten to roll back the gains made under millennium development goals. The situation is further complicated by Africa's fast-growing population that requires more resources to support itself, thus calling for efforts in building resilience against environmental shocks. As such, there is an urgent need for collective efforts in drought adaptation and mitigation to reduce the impacts of drought on agriculture, ecosystems, and human well-being. Hence, understanding the spatiotemporal variability of drought in Africa is essential to provide accurate and reliable information for decision-makers to develop effective adaptation strategies.

One of the major challenges in understanding drought variability in Africa is the limited observed station data [6], particularly in arid and semiarid lands (ASALs). This compromises drought studies, making monitoring and predicting drought occurrence and variability challenging. Satellite estimates have become increasingly important in filling data gaps [7]. Furthermore, initiatives such as the Enhancing National Climate Services (ENACTS) and EUMETSAT Africa Forum are working with national meteorological services to address this shortcoming and to migrate Africa to the latest satellite data use [6].

Studies of meteorological drought variability using multisource datasets (such as station-based, satellite-based, and reanalysis data) are important in addressing the data constraint that is common across Africa. Using various data sources to provide a more comprehensive picture of drought patterns allows for more reliable and accurate assessments of drought variability, and reduces the biases resulting from relying on a single or a few datasets [8,9]. This approach can help bridge the gap between scientific research and practical applications by providing decision-makers with more accurate and reliable information to develop effective drought mitigation and adaptation strategies. In addition, researchers also employ climate models to understand historical and projected drought patterns and characteristics.

The Greater Horn of Africa is one of the continent's most prone areas to drought [10] and has recently received considerable scientific and humanitarian attention [11], having five-consecutive failed rain seasons. The region's precipitation is on a downward trend [12,13], with strong variability in seasonal, annual, and decadal precipitation and an increasing trend in droughts [14]. The region and the Sahel have recorded the most prolonged and intense droughts across the continent for the period 1900–2013 [15]. Haile et al. [16] reported an overall increasing drought tendency across the Horn of Africa from 1964 to 2015. In a recent study, Omondi and Lin [13] investigated the trend of drought characteristics over East Africa in the last 120 years. The study equally reported an increase in drought area extent after the 1980s and linked it to the general increase in temperature and potential evapotranspiration.

West Africa's climate varies highly due to the influence of the Sahara and the Atlantic Ocean. The Sahel experienced severe droughts in the 1970s and 1980s [17]. Recent studies have observed moderate to severe droughts from 1989 to 2019 in West Africa [18,19]. According to Addi et al. [19], the standardized precipitation index (SPI) in Accra, Ghana, reduced significantly during the November–March dry season, indicating increased drought trends from 1980 to 2014. North Africa (consisting of the Mediterranean and Sahara regions) recorded multiyear droughts that add stress to an already water-strained arid land, posing a great challenge to agriculture [20], forcing farmers to tap into groundwater to irrigate crops. Belhassan [20] reported more widespread, prolonged, and frequent droughts in Northern Africa in the recent four decades, attributing it to climate variability.

Southern Africa has witnessed droughts in recent years following a reduction in precipitation in the region [1,21]. Nxumalo et al. [21] investigated the variability of meteorological drought in South Africa and its impact on wheat farming. The study noted that

frequent droughts strongly impact the country's western part and dominate the coastal areas. Pascale et al. [22] projected an increase in drought in the 21st century in South Africa. They noted that human-driven activities had increased the probability of the 2015–2017 precipitation deficit and the associated drought by a factor of five to six.

This study analyses the spatial and temporal variability of meteorological drought and its characteristics across Africa using multisource datasets. The reliance on multiple datasets and providing a comprehensive study across Africa has not been done in previous studies. Additionally, this study analyses different levels of droughts over Africa, providing a continental-scale understanding of drought variability and allowing for regional intercomparison of drought variability. The significance of this study lies in the use of multiple datasets, which is crucial for reducing biases [9]. The results of this study provide critical information for identifying and implementing relevant adaptation measures and can serve as a reference for model evaluation and projection studies, making it a valuable contribution to the field of drought research.

2. Study Area, Data, and Methods

2.1. Study Area

The African continent has a diverse landscape, reaching up to 5895 m above sea level at its highest point (Mount Kilimanjaro in Tanzania). The continent is dotted with numerous rivers and lakes, while its periphery is bordered by vast water bodies: the Atlantic Ocean to the west, the Indian Ocean to the east, and the Mediterranean and the Red Seas to the north. The water bodies play a major role in influencing meteorological conditions in various parts of Africa [23,24]. The latest climatological demarcation for Africa [25] divides the continent into nine climate subregions, namely, Mediterranean (MED), Sahara (SAH), Western Africa (WAF), Central Africa (CAF), Northern Eastern Africa (NEAF), Southern Eastern Africa (SEAF), Western Southern Africa (WSAF), Eastern Southern Africa (ESAF), and Madagascar (MDG) (Figure A1). This study analyses drought conditions based on these demarcations.

The continent's precipitation variability is strongly influenced by teleconnections, mainly ENSO. The intertropical convergence zone (ITCZ) mainly influences precipitation seasonality; precipitation to the northern hemisphere (NH) during boreal summer (June, July, and August; JJA) and to the southern hemisphere (SH) during boreal winter (December, January, and February; DJF) [26], and twice across the equator. This leads to two wet seasons a year in equatorial Africa during the boreal spring (March, April, and May; MAM), and autumn (September, October, and November; SON). However, changes in the onset and cessation of the rainy seasons, and the distribution and intensity of precipitation result in dry spells and drought episodes of varying intensity and severity in different parts of the continent [27]. In addition, shifts in large-scale atmospheric circulation contribute to distinct precipitation patterns [28]. It is observed that these changes have become erratic and frequent in recent decades [1].

2.2. Data

Each precipitation product has its strengths and weaknesses in reproducing mean and extreme precipitation [29]. This study considers three data types: gauge-based, satellite-based and reanalysis. Gauge-based data are usually regarded as "ground truth". However, the weather/gauge stations are of low density and spatially unevenly distributed in most areas across Africa, especially in the sub-Saharan region. In addition, many weather stations tend not to be continuously operational due to poor maintenance of the data recording equipment [30]. The variation in the number of gauge stations with time affects, for instance, the coherence of results of precipitation trends, thus limiting the quality of the observed data [31–33]. Furthermore, a considerable challenge is that observed datasets from the few stations in the sub-Saharan region tend to be so expensive to be acquired since they are hardly shared with researchers to support scientific research [34]. Thus, satellite and reanalysis datasets remain accessible sources of precipitation products. Satellite-based

datasets generally have higher resolution, thus providing an alternative data source over regions with sparsely-distributed weather stations [35]. It should be noted that some satellite datasets incorporate ground observations in their data [35,36]. Reanalysis data offers improved model estimates without spatial and temporal gaps using data assimilation techniques to combine forecast model outputs with observations. Thus, their applicability in regions with scarce data is vital [37,38].

This study uses daily precipitation datasets from the Frequent Rainfall Observations on GridS (FROGS) database. The FROGS project collects observed precipitation datasets from different sources and makes them available in a uniform format and at a uniform spatial resolution to facilitate research involving those datasets and their applications [29]. The project's products are processed from their native resolutions to a $1^\circ \times 1^\circ$ resolution grid using a bilinear regridding function.

Since the datasets have varying time spans, this study considers a common period of 1983–2014 in order to have the longest period with the maximum number of datasets possible. Nineteen (19) datasets (Table 1) have data covering these 32 years. The daily data are converted to monthly-accumulated precipitation amounts and used for further analyses.

Table 1. List of datasets used in this study was downloaded from FROGS. The datasets are categorised under station-based data, satellite-based data, and reanalysis data. All datasets are regridded by FROGS to a $1^\circ \times 1^\circ$.

Category	No.	Dataset	Temporal Coverage	Native Resolution	References
Station-based	1	CPC_v1.0	1979–2020	$0.5^\circ \times 0.5^\circ$	[39]
	2	GPCC_FDD_v2018	1982–2016	$1^\circ \times 1^\circ$	[40]
	3	GPCC_FDD_v2020	1982–2019	$1^\circ \times 1^\circ$	[41]
	4	REGEN_ALL_2019	1950–2016	$1^\circ \times 1^\circ$	[42]
	5	REGEN_LONG_2019	1950–2016	$1^\circ \times 1^\circ$	
Satellite-based	6	ARC2	1983–2020	$0.1^\circ \times 0.1^\circ$	[43]
	7	CHIRP_v1.0	1981–2020	$0.05^\circ \times 0.05^\circ$	[44]
	8	CHIRPS_v2.0	1981–2020	$0.25^\circ \times 0.25^\circ$	[45]
	9	PERSIANN_CCS_CDR	1983–2020	$0.04^\circ \times 0.04^\circ$	[46]
	10	PERSIANN-CDR_v1_r1	1983–2020	$0.25^\circ \times 0.25^\circ$	[47]
	11	TAMSAT_v2	1983–2017	$0.0375^\circ \times 0.0375^\circ$	
	12	TAMSAT_v3	1983–2020	$0.0375^\circ \times 0.0375^\circ$	
Reanalysis	13	CFSR	1979–2019	$0.5^\circ \times 0.5^\circ$	[48]
	14	ERA5	1979–2020	$0.25^\circ \times 0.25^\circ$	[49]
	15	ERA-I	1979–2018	$0.75^\circ \times 0.75^\circ$	[50]
	16	GSPW3	1901–2014	$0.25^\circ \times 0.25^\circ$	[51]
	17	JRA-55	1958–2019	$0.5625^\circ \times 0.5625^\circ$	[52]
	18	MERRA1	1979–2015	$0.25^\circ \times 0.25^\circ$	[53]
	19	MERRA2	1980–2019	$0.625^\circ \times 0.5^\circ$	[54]

2.3. Methods

The SPI and drought characteristics are first computed for each dataset (Table 1); then the ensemble mean of the datasets is calculated and analysed.

2.3.1. Standardized Precipitation Index

Scientists have developed various indices to characterise drought, each with unique attributes, advantages, and disadvantages. In this study, rather than evaluating the ability of various drought indicators, we focus on understanding drought characteristics in Africa.

The SPI [55,56] is among the most used indices for assessing drought. It specifically addresses the intensity of meteorological drought [55]. Meteorological drought is a precipitation deficit relative to the expected amount for a specific location and period of time which negatively impacts water supply and agricultural production. The precipitation deficit is a fundamental, intuitive metric for drought. However, interpreting the magnitude

of the precipitation deficit can be challenging because the precipitation average varies widely over geographical regions and temporal scales. Furthermore, the precipitation deficit/excess is evaluated relative to some climatological norm for the location. Thus, the challenge of drought definition lies not in the raw measurement of hydrometeorological data but in the objective assessment of the observations. SPI addresses this challenge by comparing the precipitation total for a chosen interval against a cumulative probability distribution for the precipitation data over identical time intervals.

The SPI assigns a single numeric value (number of standard deviations that the observed value would deviate from the long-term mean) to the precipitation that can be compared across regions with markedly different climates for any accumulation timescale (e.g., 3, 6, or 12 months). The negative (positive) SPI values correspond to drier (wetter) periods than normal. The magnitude of the departure from the mean is a probabilistic measure of the severity of a wet or dry event.

In comparison to other indices such as the Palmer severity drought index, SPI uses precipitation only and characterises drought or abnormal wetness at different time scales that correspond to the time availability of different water resources, such as soil moisture, snowpack, groundwater, river discharge, and reservoir storage. Thus, SPI is more comparable across regions with different climatic conditions than other indices. However, the index does not account for evapotranspiration as a measure of water supply only, which limits its ability to capture the effect of increased temperatures (associated with climate change) on moisture demand and availability. The negative range of SPI is arbitrarily divided into four categories (Table 2). Drought variability analyses are conducted for all drought months and for moderate, severe, and extreme drought months.

Table 2. Classification of drought level from SPI values [55].

SPI Values	Drought Level Classification
$-1.0 > \text{SPI}$	all drought
$-1.0 \geq \text{SPI} > -1.5$	moderate drought
$-1.5 \geq \text{SPI} > -2$	severe drought
$-2.0 \geq \text{SPI}$	extreme drought

When deriving SPI, the choice of a time scale (or an aggregation level) can be linked to the relevance of the drought analysis for hydrometeorological applications. This work focuses on the 3-month time scale (SPI-3) because we are interested in meteorological drought which is relevant for rainfed agricultural practices. On short timescales, SPI is closely related to soil moisture, while at longer timescales (e.g., 6–9 and 12–24 months), SPI can be related to groundwater and reservoir storage, which is relevant to water resources or hydrological applications. As mentioned in Section 2.1, depending on the subregion of the study area, the wet and dry seasons can occur during DJF, MAM, JJA, and SON seasons. For instance, JJA and DJF are dry seasons in areas along the equator [12,57]. Therefore, the results of our analysis based on a 3-month time scale are relevant for monitoring changes in soil moisture conditions due to seasonal variation in rainfall.

A 3-month SPI compares the precipitation for three consecutive months with the same three consecutive months during all the previous years of available data. The SPI (Equation (1)) at these time scales reflects precipitation patterns.

$$\text{SPI} = \frac{(\text{PRE} - \bar{\text{PRE}})}{\sigma_{\text{PRE}}} \quad (1)$$

where PRE is monthly-accumulated precipitation, $\bar{\text{PRE}}$ is mean precipitation, and σ_{PRE} is the standard deviation of precipitation.

SPI-3 is computed using the in-built function in the NCAR command language (NCL). The NCL calculates SPI by fitting the monthly precipitation values to a gamma distribution. Then, a transformation is performed such that the derived SPI values follow a normal

distribution. It should be noted that months 1 to 2 have no values for SPI-3 since the 3-month period starts on month 3.

The cumulative precipitation ($X_{i,j}^t$) for the j^{th} month in the i^{th} year based on the time scale (t) is given by Equation (2):

$$X_{i,j}^t = \sum_{k=0}^{t-1} (x_{i,j-k}) \quad (2)$$

The next step involved fitting the cumulative density function (CDF) of the gamma distribution to $X_{i,j}^t$ using Equation (3). According to Gutmann [58], the distribution (Γ being the gamma function) is ordinarily applied in SPI calculations directly or in its location parameter extended version, the Pearson type III distribution.

$$g(x) = \frac{1}{\beta^\alpha \Gamma(\alpha)} x^{\alpha-1} e^{-\frac{x}{\beta}} \quad (3)$$

where α and β are shape and scale parameters, respectively, and x is the precipitation amount (where $x > 0$). $\Gamma(\alpha)$ is the gamma function. The gamma distribution optimally fits with long-term precipitation trends [59]. According to Wilks [60], α and β can be better estimated by using an iterative procedure in some conditions.

The CDF ($G(x)$) can be calculated as (Equation (4)):

$$G(x) = \int_0^x g(x) dx \quad (4)$$

To take into account the possibility of having zeros in the precipitation series, the CDF of the gamma distribution with $x = 0$ can be modified as (Equation (5)):

$$H(x) = q + (1 - q) G(x) \quad (5)$$

where q refers to the probability of zero precipitation.

The last step involves normalising the cumulative probability distribution to produce the SPI (Equation (6)).

$$SPI = \begin{cases} -\left(s - \frac{c_0+c_1s+c_2s^2}{1+w_1s+w_2s^2+w_3s^3}\right), & s = \sqrt{\ln\left(\frac{1}{(H(x))^2}\right)} \\ & \text{for } 0 < H(x) < 0.5 \\ s - \frac{c_0+c_1s+c_2s^2}{1+w_1s+w_2s^2+w_3s^3}, & s = \sqrt{\ln\left(\frac{1}{(1.0-H(x))^2}\right)} \\ & \text{for } 0.5 < H(x) < 1 \end{cases} \quad (6)$$

where $c_0 = 2.515517$, $c_1 = 0.802853$, $c_2 = 0.010328$, $w_1 = 1.432788$, $w_2 = 0.189269$, and $w_3 = 0.001308$.

2.3.2. Drought Characteristics

Drought variability is evaluated using several drought characteristics. Table 3 lists the drought characteristics considered in this study and their computation equation [61]. The characteristics are computed for each drought level (Table 2).

Table 3. Drought characteristics used in the study, where drought months are months with $SPI \leq -1$. D: drought duration (month); d_e : duration of e^{th} drought event; e: number of drought events; n: number of drought months; F: frequency (%); N: total number of months; I: drought intensity; SPI_i : SPI value during i^{th} drought month; S: drought severity; A: drought area (%); p: number of pixels with $SPI \leq -1$; and P: total number of pixels.

Drought Characteristic	Equation
Drought duration	$D = \frac{\sum_{e=1}^n d_e}{e}$
Drought frequency	$F = \frac{n}{N} \times 100$
Drought intensity	$I = \frac{1}{n} \sum_{i=1}^n SPI_i$
Drought severity	$S = D \times I$
Drought impact area	$A = \frac{\sum_{i=1}^n P}{P} \times 100$

2.3.3. Trend Analysis

The magnitude of linear change in the SPI-3 time series is calculated using the Theil–Sen slope estimator [62]. We also use the nonparametric Mann–Kendall (MK) test [63,64] to estimate the normalised test statistics, Z, of the time series, which represents the trend of the SPI-3 change. The $Z < 0$ and $Z > 0$ indicate decreasing and increasing trends, respectively. We use a Student's *t*-test to calculate the statistical significance of the trend at a 95% confidence level. Several of the existing literature have applied the Theil–Sen slope estimator and the MK test (e.g., [4,65–69]).

3. Results

3.1. Spatial and Temporal Analysis of Drought Months

Figure 1 shows the spatial distribution of SPI-3 for the different categories of drought months (Table 2) over Africa from 1983 to 2014. The results reveal that although drought occurs in most parts of the continent, it is more common in the equatorial regions. These are the regions with more negative SPI values. Figure 1a shows SPI values with more negative values in WAF, CAF, NEAF, and parts of SEAF for all months, whereas Eastern SAH and WSAF show less negative SPI values indicating less dry conditions. The same is observed, though on a larger scale, during moderate, severe, and extreme drought periods, with SPI index values going as low as -2.7 during extreme drought months (Figure 1d). The most prevalent drought in the region is moderate to severe, covering most of Africa except for SAH and a few places around WSAF, where SPI values are less negative (yellowish colour). Extreme drought is pronounced in the equatorial region. Parts of NEAF and SEAF record more drought conditions. MDG and most of ESAF experience more moderate to severe drought than other drought classes.

A comparison of all drought months, and moderate, severe, and extreme drought months spatial distribution demonstrates that all drought months do not depict the drought distribution and intensity of the different drought levels. For example, more negative SPI values over CAF are more pronounced during moderate and severe droughts than during extreme drought months. Therefore, it is important to analyse drought at different drought levels.

Figure 2 displays the interannual variability of SPI-3 for all drought months and different drought categories across the nine regions of Africa. Drought variability affects planning, mitigation actions, and resilience of the communities to adapt to the changing drought situation. The interannual variability of drought months differs across all regions. The highest interannual variability is recorded during the extreme drought periods (red line). Moderate drought months (green line) have the least interannual variability. A few years stand out with the largest variability across the regions, such as 1988, 2003, and 2013. Extreme drought events are observed in the MED region during 1996, while SAH and WAF experience extreme droughts in 1985 and 1990, respectively. NEAF and WAF experience multiple occurrences of extreme droughts during the study period.

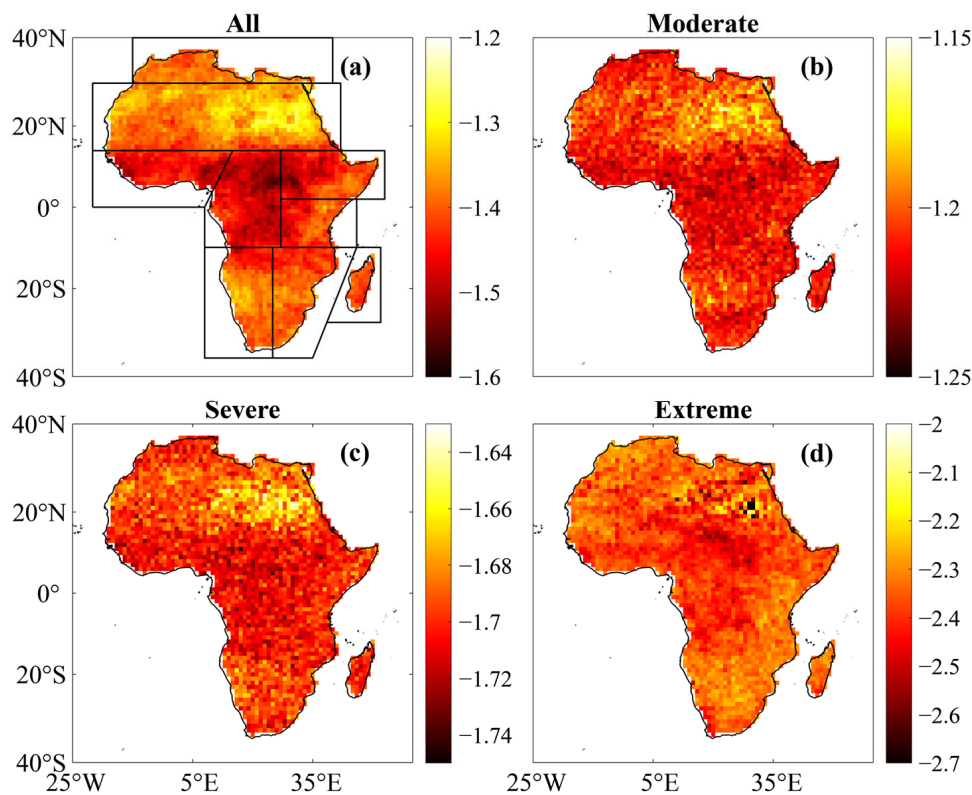


Figure 1. Spatial distribution of SPI-3 ensemble mean over Africa during 1983–2014 from the gauge-based, satellite-based, and reanalysis data for different drought categories. (a) All; (b) moderate; (c) severe; and (d) extreme drought. The demarcations in (a) delineate the climate subregions of Africa. Note that the colour bars have different ranges.

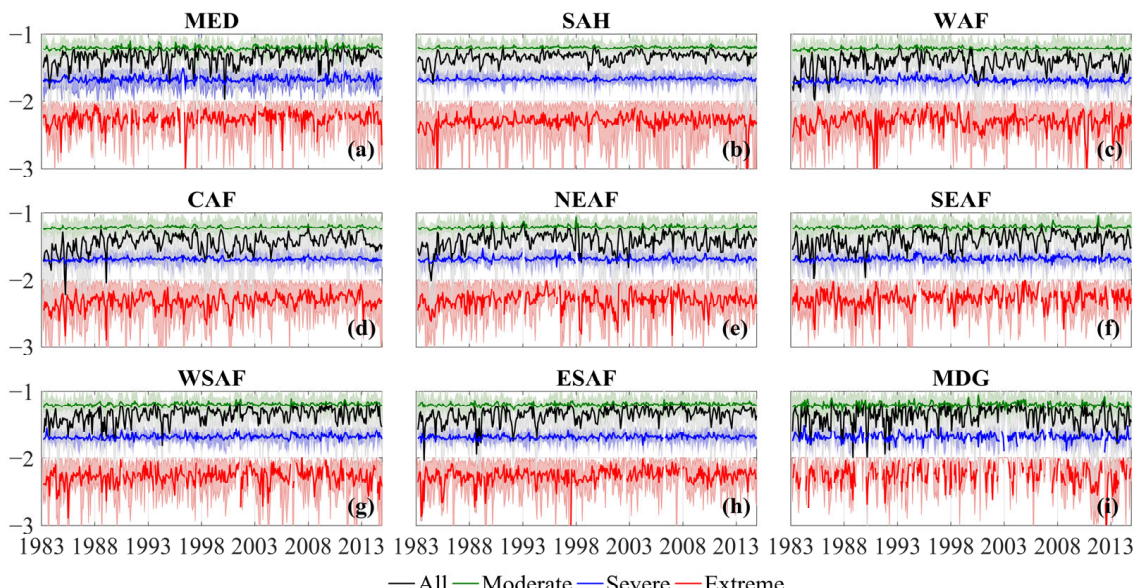


Figure 2. Interannual variability of drought from the ensemble mean of SPI-3 over the subregions of Africa during 1983–2014. (a) MED; (b) SAH; (c) WAF; (d) CAF; (e) NEAF; (f) SEAF; (g) WSAF; (h) ESAF; and (i) MDG. Black, red, blue, and green represent all, moderate, severe, and extreme drought months, respectively. The shadings are the maximum and minimum SPI values from the individual datasets.

Table 4 presents the trend analysis of SPI for all drought months, and moderate, severe, and extreme drought months over the subregions of Africa. The analysis reveals an increasing trend in SPI for mostly all drought categories, especially in the tropical areas of WAF, CAF, SEAF, and ESAF. Analysing the magnitude of linear change (slope), CAF shows the largest positive change (0.322) for all drought months, while the region with the least positive change is MDG (0.089). For moderate droughts, MED and WSAF present the largest positive change (0.061). These values indicate an increase in moderate droughts over time in these regions. The region with the lowest linear change for moderate droughts is MDG (0.016), indicating a slight increase in moderate droughts over time. WSAF shows the highest increasing change for severe droughts (0.073), while MDG shows a decreasing change of -0.028 , indicating a slight decrease in severe droughts over time. For extreme droughts, CAF displays the largest increasing linear change of 0.252, while WAF and MDG show a decrease in extreme drought (-0.028 and -0.035 , respectively).

Table 4. Trend analysis of drought months over the climate subregions of Africa using the modified Mann—Kendall test and the Theil-Sen slope estimator. Slope is the magnitude of linear-trend change (scale: $\times 10^{-3}$), and positive and negative values of Z represent increasing and decreasing trends, respectively, and p is the statistical significance at a 95% confidence level.

		MED	SAH	WAF	CAF	NEAF	SEAF	WSAF	ESAF	MDG
All	Slope	0.290	0.222	0.322	0.377	0.232	0.358	0.337	0.349	0.089
	Z	4.027	5.538	0.900	3.458	1.518	4.309	6.755	5.016	1.215
	p	0.000	0.000	0.368	0.001	0.129	0.000	0.000	0.000	0.224
Moderate	Slope	0.061	0.036	0.039	0.031	0.035	0.043	0.061	0.051	0.016
	Z	4.782	5.007	3.220	10.213	2.786	3.762	5.739	4.774	1.157
	p	0.000	0.000	0.001	0.000	0.005	0.000	0.000	0.000	0.247
Severe	Slope	0.046	0.032	0.023	0.032	0.025	0.026	0.073	0.050	-0.028
	Z	1.949	4.821	1.180	2.795	1.439	2.600	4.543	4.289	-0.696
	p	0.051	0.000	0.238	0.005	0.150	0.009	0.000	0.000	0.486
Extreme	Slope	0.113	0.154	-0.028	0.252	0.083	0.161	0.093	0.240	-0.035
	Z	2.864	4.995	-1.065	3.907	0.539	3.183	1.677	2.885	-0.103
	p	0.004	0.000	0.287	0.000	0.590	0.001	0.093	0.004	0.918

Analysing the trend in SPI (Z), WSAF shows the largest increasing trend for all drought months (6.755), while WAF shows the smallest increasing trend (0.900), followed by MDG (1.215). CAF shows the highest increasing trend for moderate drought (10.213), while SAH shows the largest increasing trend for severe (4.821) and extreme drought (4.995). While different regions stand out as the area with the highest increasing trend for different drought categories, MDG has the smallest increase for moderate drought (1.157) and decreasing trends for severe (-0.696) and extreme (-0.103) drought.

The trend analysis for all drought months and different drought categories over different regions of Africa shows varying levels of increasing or decreasing drought episodes over time.

3.2. Analysis of Drought Characteristics

This section presents the spatiotemporal characteristics of drought for all drought months and moderate, severe, and extreme drought months.

3.2.1. Drought Duration

Figure 3 shows the spatial distribution of drought duration over Africa. For all drought months, the longest drought duration is observed along the equatorial region, except the eastern part of NEAF. This observation is also true during extreme drought events, only that the area during extreme drought events expands to cover more areas along the tropical region. In contrast, CAF experiences long drought duration for all drought months and

extreme drought months, while the Eastern SAH experiences long drought duration for moderate, severe, and extreme drought months. Extreme drought months exhibit large values within the equatorial regions (WAF, CAF, NEAF, and SEAF). In contrast, WSAF and ESAF exhibit the shortest extreme drought conditions, potentially due to seasonal precipitation patterns that modulate drought conditions frequently. Overall, drought duration varies greatly across different regions of Africa with some areas experiencing longer and more severe droughts than others.

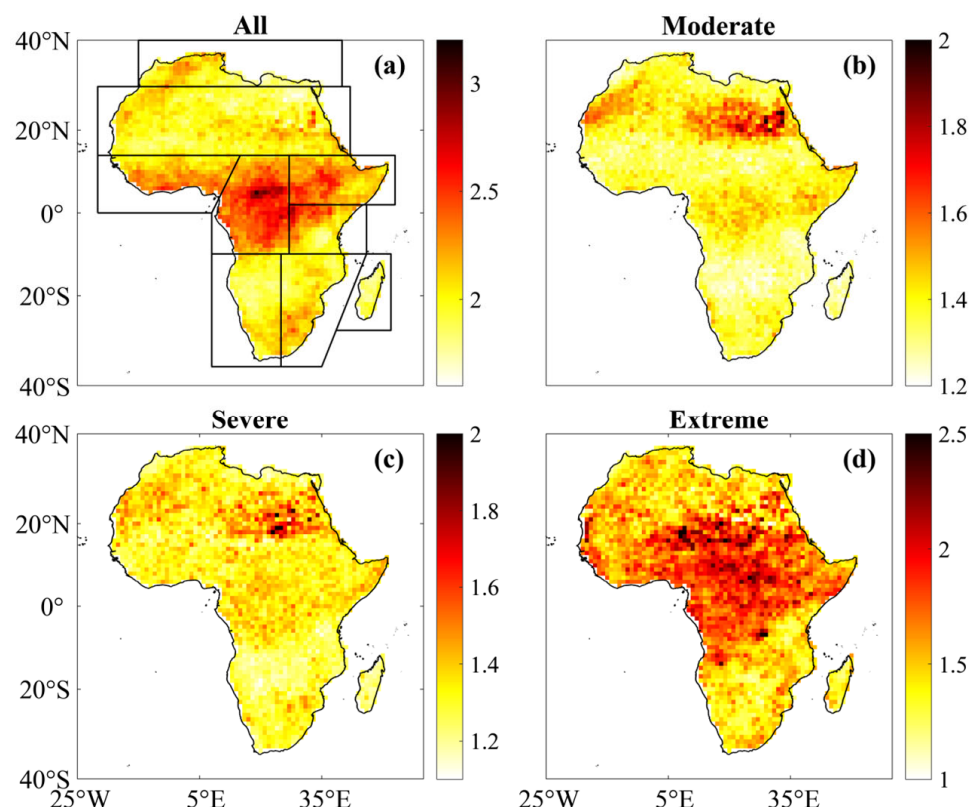


Figure 3. Spatial distribution of drought duration (months) over Africa during 1983–2014 averaged from the gauge-based, satellite-based, and reanalysis data for different drought categories. **(a)** All; **(b)** moderate; **(c)** severe; and **(d)** extreme drought. The demarcations in **(a)** delineate the climate subregions of Africa.

Table 5 shows the drought duration averaged over different regions of Africa for different drought categories. The average drought duration for all drought months is longer in CAF, WSAF, and NEAF than in other regions. MDG presents the shortest drought duration for all drought categories (1.29, 1.23, and 1.38 months for moderate, severe, and extreme drought, respectively). On the other hand, SAH displays the longest duration for moderate and severe drought (1.44 and 1.37 months, respectively), while CAF presents the longest duration for extreme drought (1.85 months). SAH, WAF, CAF, and NEAF generally have longer drought durations. Overall, the duration of severe drought is shorter (average of 1.31 months) compared to moderate and extreme drought (average of 1.36 and 1.57 months, respectively), suggesting that moderate and extreme droughts tend to last longer than severe droughts.

Table 5. Drought duration (months year⁻¹) averaged over the climate subregions of Africa for all, moderate, severe, and extreme drought months during 1983–2014. Mean represents the ensemble mean of all datasets, and max and min are the upper and lower bound of the uncertainty range, respectively, obtained from the maximum and minimum duration from the individual datasets.

	MED	SAH	WAF	CAF	NEAF	SEAF	WSAF	ESAF	MDG
All	Max	2.11	2.39	2.69	3.87	2.95	2.57	2.26	2.27
	Mean	2.03	1.97	2.20	2.39	2.24	2.15	1.98	2.05
	Min	1.88	1.77	1.88	1.97	1.94	1.91	1.72	1.72
Moderate	Max	1.40	1.72	1.51	1.59	1.48	1.50	1.40	1.41
	Mean	1.34	1.44	1.35	1.38	1.39	1.36	1.32	1.34
	Min	1.30	1.31	1.27	1.26	1.30	1.27	1.27	1.26
Severe	Max	1.33	1.52	1.44	1.59	1.50	1.44	1.35	1.39
	Mean	1.28	1.37	1.31	1.35	1.34	1.31	1.26	1.29
	Min	1.24	1.27	1.20	1.25	1.25	1.22	1.22	1.21
Extreme	Max	1.59	2.07	2.41	2.70	2.07	1.74	1.58	1.66
	Mean	1.40	1.60	1.71	1.85	1.72	1.57	1.45	1.44
	Min	1.31	1.45	1.35	1.53	1.39	1.39	1.26	1.24

3.2.2. Drought Events

Figure 4 shows the distribution of drought events over Africa. Eastern SAH has the lowest number of events, while regions such as MED, WAF, SEAF, WSAF, ESAF, and MDG have a high number of drought events. However, these regions also have short drought durations (Figure 3). In addition, CAF and NEAF have a low number of events but with a longer duration. Overall, the number of drought events varies across regions. The results suggest that extreme droughts are the most persistent and impactful over the equatorial region, with long durations (Figure 3d) and high numbers of events (Figure 4d). Despite having a generally long drought duration, Eastern SAH has a low number of drought events. In contrast, the low number of events in CAF, but with a long duration for all and extreme drought months, poses a high risk to the region's agriculture and water resources.

Table 6 shows the drought events averaged over different regions of Africa for different drought categories. The number of drought events decreases from moderate to severe and extreme droughts. For all drought months, MDG and CAF present the highest and lowest number of drought events (30.39 and 24.05 events, respectively). Compared with the drought duration (Table 5), the results indicate a high number of drought occurrences in MDG but with a short duration, while the opposite is noted over CAF. For moderate drought, the number of drought events ranges from 20.53 events (SAH) to 26.31 events (MDG). For severe droughts, the highest and lowest number of drought events occur in MED (12.23 events) and SAH (8.29 events), respectively. WAF shows the highest number of drought events (5.11 events) for extreme drought, while SAH shows the lowest number of events (3.09 events). These results suggest that drought events are most frequent in regions such as MDG and MED and that most regions experience more moderate drought (average of 24.09 events).

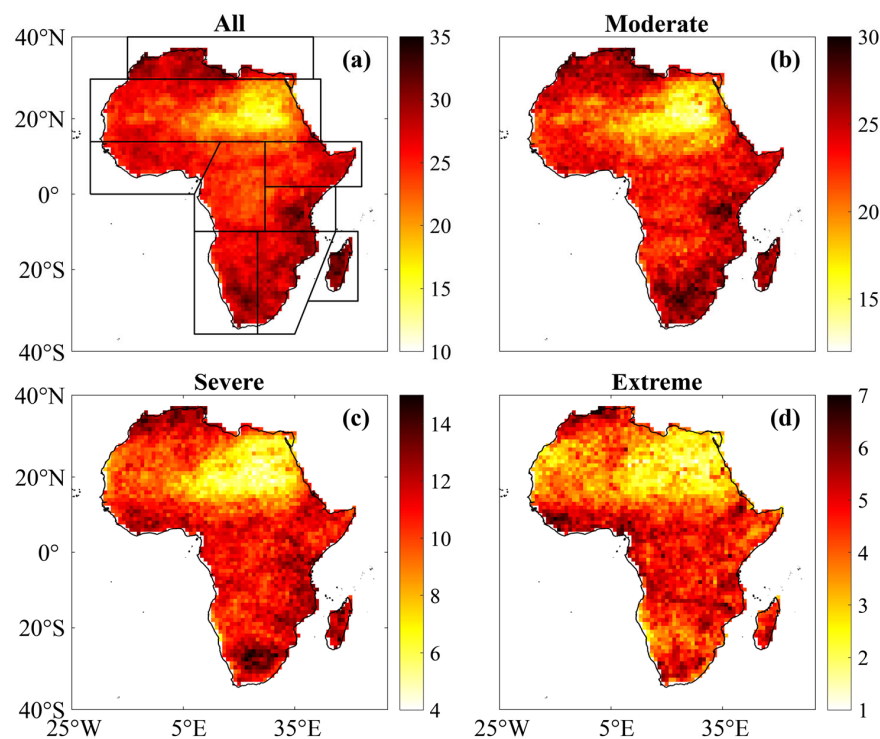


Figure 4. Spatial distribution of drought events over Africa during 1983–2014 averaged from the gauge-based, satellite-based, and reanalysis data for different drought categories. (a) All; (b) moderate; (c) severe; and (d) extreme drought. The demarcations in (a) delineate the climate subregions of Africa.

Table 6. Drought events (year^{-1}) averaged over the climate subregions of Africa for all, moderate, severe, and extreme drought months during 1983–2014. Mean represents the ensemble mean of all datasets, and max and min are the upper and lower bound of the uncertainty range, respectively, obtained from the maximum and minimum duration from the individual datasets.

	MED	SAH	WAF	CAF	NEAF	SEAF	WSAF	ESAF	MDG
All	Max	30.62	34.29	30.90	28.78	28.67	29.76	31.42	30.88
	Mean	29.21	22.61	25.99	24.05	25.64	27.72	27.80	28.35
	Min	25.69	12.22	21.56	17.87	22.36	24.86	24.97	24.45
Moderate	Max	28.00	31.57	26.20	26.60	26.91	27.23	29.17	28.88
	Mean	25.97	20.53	23.09	22.36	23.41	25.19	24.54	25.46
	Min	22.14	10.87	19.58	18.36	21.39	22.48	22.18	20.48
Severe	Max	13.25	12.77	12.93	12.23	12.44	13.04	12.84	13.04
	Mean	12.23	8.29	11.20	10.67	10.78	11.67	11.19	11.69
	Min	9.09	4.18	8.92	8.34	7.43	8.22	8.01	8.41
Extreme	Max	6.58	5.17	7.06	7.78	6.38	7.37	5.75	6.45
	Mean	4.85	3.09	5.11	4.74	4.43	4.75	4.47	4.61
	Min	2.23	1.70	3.29	2.18	1.65	1.79	2.37	2.14

3.2.3. Drought Frequency

Figure 5 shows the drought frequency in Africa. The drought frequencies of moderate, severe, and extreme drought months reflect distribution from all drought months. In addition, the spatial distribution of drought events and frequency generally agrees. In analysing the frequency of drought events in Africa, we find that the lowest frequency occurs in the Eastern SAH and WSAF. This is interesting because WSAF is known to be a dry region [68]. The results indicate that although this region is arid, it does not experience many drought occurrences.

The spatial distributions show high frequency over most regions of Africa (including MED, WAF, CAF, NEAF, SEAF, Southern WSAF, ESAF, and MDG). In addition, the southern tip of Africa displays a high frequency of moderate and severe droughts. However, compared to drought duration (Figure 3) and events (Figure 4), it is evident that although they have a high drought frequency, the events have a short duration. This implies that the regions experience frequent droughts but with short-term impacts.

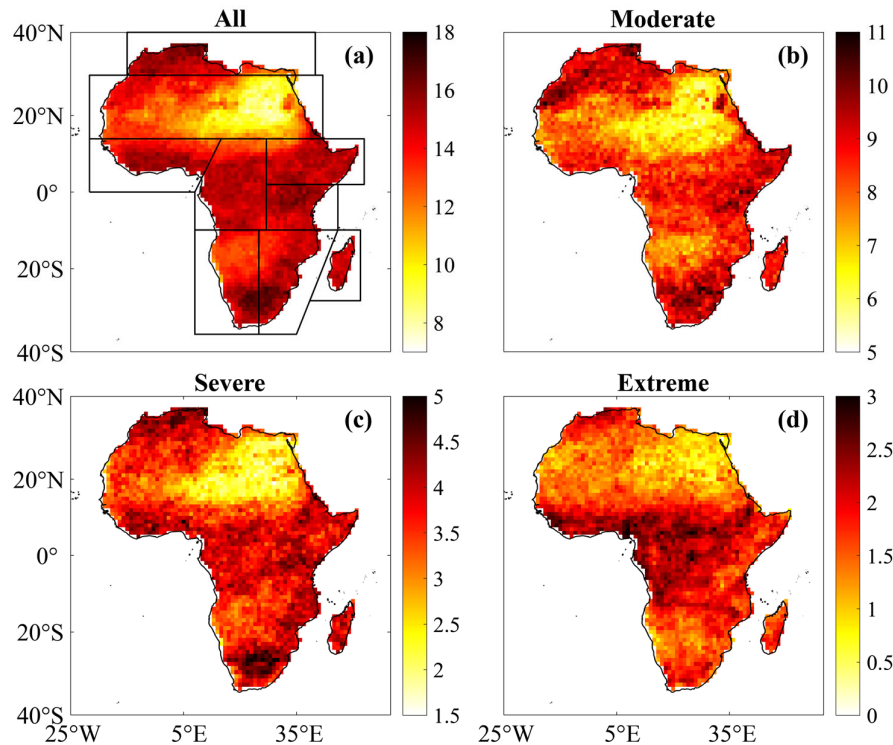


Figure 5. Spatial distribution of drought frequency (%) over Africa during 1983–2014 averaged from the gauge-based, satellite-based, and reanalysis data for different drought categories. (a) All; (b) moderate; (c) severe; and (d) extreme drought. The demarcations in (a) delineate the climate subregions of Africa.

Table 7 shows the drought frequency averaged over different regions of Africa for different drought categories during 1983–2014. Drought frequency for moderate, severe, and extreme droughts ranges from 7.74 (SAH) to 9.13% (MED), 2.93 (SAH) to 4.10% (MED), and 1.23 (SAH) to 2.24% (CAF), respectively. The analysis of drought frequency across Africa reveals some interesting patterns. Specifically, the results show that SAH has the lowest drought frequency for all categories (7.74, 2.93, and 1.23% for moderate, severe, and extreme droughts, respectively), while MED has the highest frequency for all categories (9.13 and 4.10% for moderate and severe drought, respectively) except for extreme drought months (where CAF has the highest frequency of 2.24%). Compared with the drought duration results (Table 5), SAH displays longer drought durations for moderate and severe drought (1.44 and 1.37 events, respectively) and among the longest for extreme drought (1.60 events). This indicates that the drought occurrences in SAH are less frequent but with longer duration. The opposite is observed for MED. Analysing the different drought categories, the results indicate that moderate droughts are the most frequent across all regions (with an average of 8.56% per year), suggesting that although Africa is prone to drought, most droughts experienced are moderate. CAF shows a unique trend where moderate drought frequency is among the lowest (8.12%) but extreme drought frequency is the highest (2.24%).

Table 7. Drought frequency (% year⁻¹) averaged over the climate subregions of Africa for all, moderate, severe, and extreme drought months during 1983–2014. Mean represents the ensemble mean of all datasets, and max and min are the upper and lower bound of the uncertainty range, respectively, obtained from the maximum and minimum duration from the individual datasets.

	MED	SAH	WAF	CAF	NEAF	SEAF	WSAF	ESAF	MDG
All	Max	16.47	18.99	16.08	17.03	16.38	16.20	16.09	16.61
	Mean	15.39	11.75	14.63	14.49	14.60	15.24	14.30	15.03
	Min	12.96	5.67	12.78	12.21	11.86	12.98	11.85	12.39
Moderate	Max	10.14	12.86	9.50	10.45	10.14	10.52	10.40	10.30
	Mean	9.13	7.74	8.16	8.12	8.53	8.99	8.53	8.94
	Min	7.74	3.92	6.77	6.45	7.58	7.51	7.47	5.48
Severe	Max	4.42	4.57	4.23	4.78	4.47	4.39	4.23	4.46
	Mean	4.10	2.93	3.83	3.75	3.77	3.97	3.69	3.95
	Min	2.94	1.54	3.08	2.94	2.69	2.84	2.54	2.67
Extreme	Max	2.41	2.12	3.99	4.00	3.06	2.91	2.22	2.27
	Mean	1.75	1.23	2.20	2.24	1.94	1.89	1.67	1.71
	Min	0.78	0.63	1.51	0.98	0.79	0.69	0.90	0.72

3.2.4. Drought Intensity

Figure 6 shows the spatial distribution of drought intensity across Africa. Interpretation of drought intensity and severity is based on the magnitude rather than the negative sign. For instance, the more negative the value, the higher the drought intensity. The results show that drought intensity varies greatly across Africa and for different drought categories. CAF and part of WAF stand out as having high intensity for all drought months. On the other hand, WSAF and ESAF show low drought intensity for all drought months and extreme drought months. In general, extreme drought months tend to have higher intensity over the tropical regions, while higher intensities are observed over most regions of Africa, except SAH, for moderate and severe droughts. In addition, Eastern SAH consistently displays lower intensity for all drought categories.

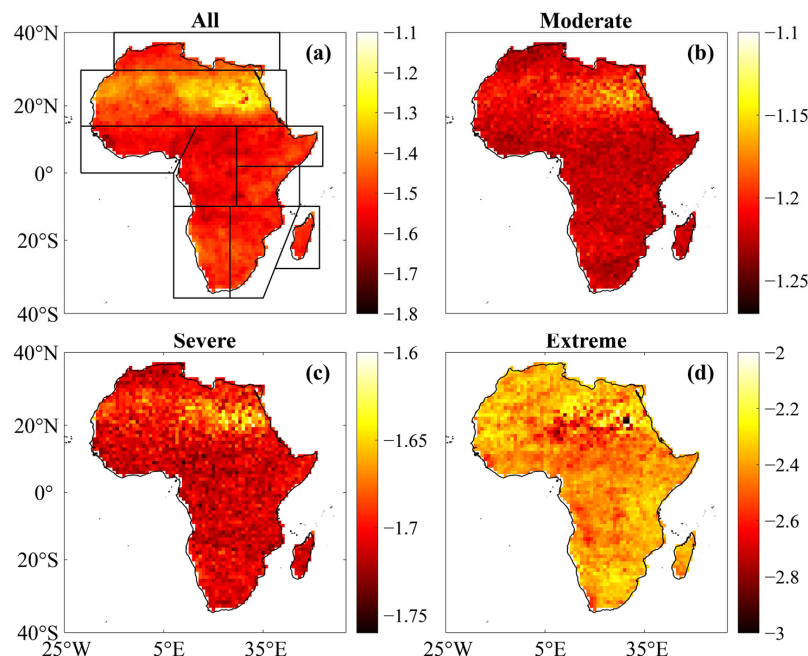


Figure 6. Spatial distribution of drought intensity over Africa during 1983–2014 averaged from the gauge-based, satellite-based, and reanalysis data for different drought categories. (a) All; (b) moderate; (c) severe; and (d) extreme drought. The demarcations in (a) delineate the climate subregions of Africa.

Table 8 shows the drought intensity averaged over different regions of Africa. The drought intensity for moderate, severe, and extreme drought months ranges from -1.20 to -1.22 , -1.69 to -1.71 , and -2.36 to -2.45 (CAF), respectively. This suggests that although extreme droughts have the lowest frequency of occurrence, they have the highest impact when they do occur.

Table 8. Drought intensity (year^{-1}) averaged over the climate subregions of Africa for all, moderate, severe, and extreme drought months during 1983–2014. Mean represents the ensemble mean of all datasets, and max and min are the upper and lower bound of the uncertainty range, respectively, obtained from the maximum and minimum duration from the individual datasets.

	MED	SAH	WAF	CAF	NEAF	SEAF	WSAF	ESAF	MDG	
All	Max	-1.41	-1.29	-1.49	-1.44	-1.43	-1.38	-1.42	-1.39	-1.38
	Mean	-1.50	-1.42	-1.56	-1.56	-1.52	-1.51	-1.51	-1.50	-1.50
	Min	-1.57	-1.57	-1.71	-1.73	-1.62	-1.63	-1.58	-1.63	-1.63
Moderate	Max	-1.21	-1.17	-1.22	-1.21	-1.21	-1.21	-1.20	-1.21	-1.21
	Mean	-1.22	-1.20	-1.22	-1.22	-1.22	-1.22	-1.22	-1.22	-1.22
	Min	-1.23	-1.22	-1.23	-1.23	-1.23	-1.23	-1.23	-1.23	-1.23
Severe	Max	-1.69	-1.67	-1.70	-1.70	-1.70	-1.69	-1.69	-1.69	-1.69
	Mean	-1.71	-1.69	-1.71	-1.71	-1.71	-1.71	-1.71	-1.71	-1.71
	Min	-1.72	-1.71	-1.73	-1.73	-1.72	-1.72	-1.72	-1.73	-1.73
Extreme	Max	-2.29	-2.28	-2.38	-2.29	-2.30	-2.28	-2.34	-2.27	-2.28
	Mean	-2.36	-2.41	-2.43	-2.45	-2.43	-2.36	-2.40	-2.37	-2.39
	Min	-2.49	-2.63	-2.51	-2.79	-2.58	-2.44	-2.58	-2.48	-2.50

3.2.5. Drought Severity

The spatial distribution of drought severity over Africa (Figure 7) reveals some interesting patterns. All drought months show high severity over CAF and parts of WAF, NEAF, and SEAF, while Eastern SAH and WSAF exhibit low intensity. Moderate and severe drought months show high severity over Eastern SAH, while the rest of the continent experiences relatively much lower drought severity. Extreme drought months tend to have higher intensity over the equatorial region. MDG depicts low severity for all drought categories. The severity of drought events is consistent with duration and intensity, with regions such as CAF showing high severity due to long durations and high intensity. The severity of moderate and severe drought in Eastern SAH indicates that although the intensity over the region is lower, the drought occurrences have a long duration. These findings help identify areas of high vulnerability and aid in developing targeted drought mitigation strategies.

Table 9 shows the drought severity averaged over different regions of Africa. The results show that drought severity varies across different regions of the continent and impacts all regions of Africa. Moderate, severe, and extreme drought has the smallest and largest severity in MDG (-1.58) and SAH (-1.73), MDG (-2.10) and SAH (-2.33), and MED (-3.33) and CAF (-4.61), respectively. MDG has the lowest severity for moderate and severe droughts (and second lowest for all drought and extreme drought months), indicating that it is the region least affected by drought. On the other hand, SAH has the highest severity for moderate and severe drought months, suggesting that this region is more prone to moderate and severe droughts. Additionally, CAF has the highest severity for extreme drought months, followed by NEAF (-4.23) and WAF (-4.19), indicating that these regions are more vulnerable to extreme drought conditions. Overall, the drought severity has a consistent pattern with the drought duration (Table 5) and intensity (Table 8) results, highlighting the importance of monitoring both factors to accurately assess drought severity in Africa. The results show that droughts in Africa can have strong impacts, especially when they reach extreme drought levels. Therefore, monitoring drought conditions and implementing appropriate measures to mitigate their effects is important.

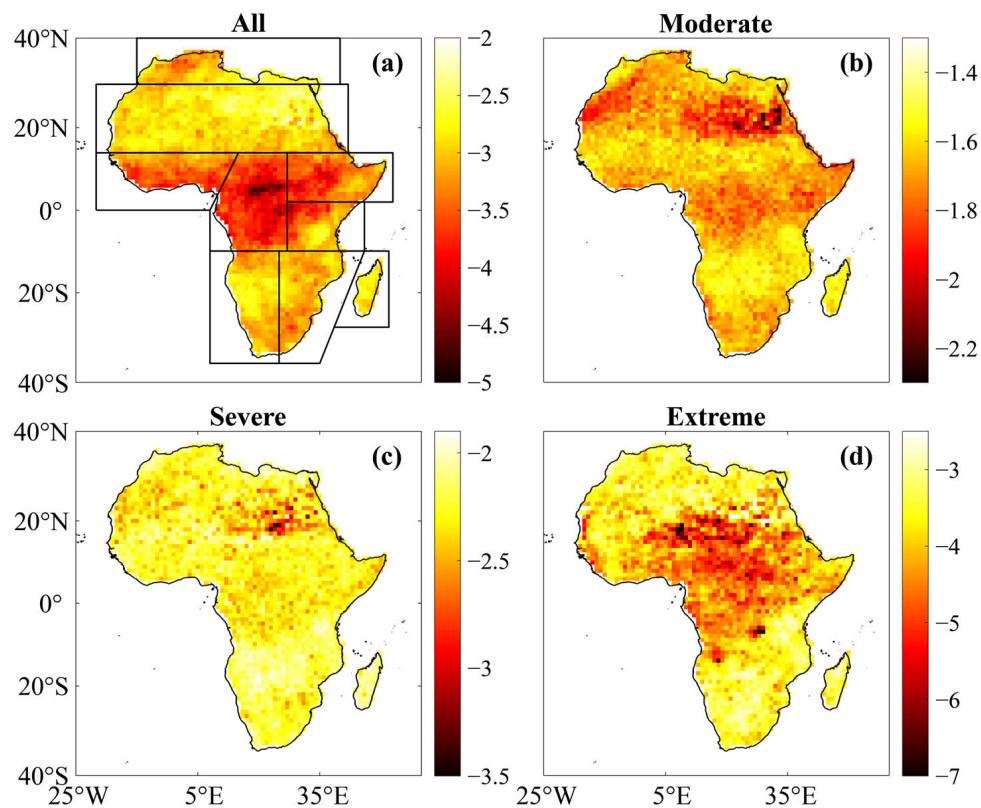


Figure 7. Spatial distribution of drought severity over Africa during 1983–2014 averaged from the gauge-based, satellite-based, and reanalysis data for different drought categories. (a) All; (b) moderate; (c) severe; and (d) extreme drought. The demarcations in (a) delineate the climate subregions of Africa.

Table 9. Drought severity (year^{-1}) averaged over the climate subregions of Africa for all, moderate, severe, and extreme drought months during 1983–2014. Mean represents the ensemble mean of all datasets, and max and min are the upper and lower bound of the uncertainty range, respectively, obtained from the maximum and minimum duration from the individual datasets.

	MED	SAH	WAF	CAF	NEAF	SEAF	WSAF	ESAF	MDG
All	Max	-2.65	-2.40	-2.93	-2.94	-2.78	-2.64	-2.45	-2.41
	Mean	-3.05	-2.82	-3.43	-3.76	-3.43	-3.27	-3.00	-3.11
	Min	-3.34	-3.37	-4.41	-6.32	-4.78	-3.99	-3.51	-3.71
Moderate	Max	-1.58	-1.60	-1.55	-1.55	-1.59	-1.57	-1.56	-1.54
	Mean	-1.64	-1.73	-1.65	-1.69	-1.70	-1.67	-1.62	-1.64
	Min	-1.70	-2.08	-1.85	-1.95	-1.81	-1.83	-1.71	-1.68
Severe	Max	-2.11	-2.14	-2.06	-2.14	-2.14	-2.13	-2.07	-2.01
	Mean	-2.20	-2.33	-2.25	-2.32	-2.29	-2.25	-2.16	-2.22
	Min	-2.29	-2.57	-2.46	-2.73	-2.56	-2.46	-2.30	-2.38
Extreme	Max	-3.07	-3.33	-3.27	-3.69	-3.30	-3.28	-2.99	-2.77
	Mean	-3.33	-3.93	-4.19	-4.61	-4.23	-3.76	-3.54	-3.49
	Min	-3.99	-5.01	-5.88	-7.25	-5.43	-4.22	-4.10	-4.26

The results demonstrate that analysing all drought months without considering the different drought categories can lead to wrong conclusions. This reflects the importance of analysing drought at different levels to better understand the situation.

3.2.6. Drought Impact Area

The drought impact area (see Table 3 for the equation) displays the percentage area of a subregion that experiences a certain level of drought.

Figure 8 shows the interannual variability of drought impact areas for all drought months. The impact of drought events on different regions of Africa shows a large variability in terms of the affected area. MDG has the largest variability (standard deviation of 13.06%), while SAH has the smallest variability (standard deviation of 7.76%). The maximum drought impact area ranges from 68.34 (ESAF) to 39.73% (CAF), while the minimum drought impact area ranges from 0.00 (MDG) to 1.14% (CAF). The mean impact area for MED, SAH, WAF, CAF, NEAF, SEAF, WSAF, ESAF, and MDG is 15.16, 11.23, 14.52, 14.67, 14.81, 15.38, 14.20, 14.97, and 14.93%, respectively.

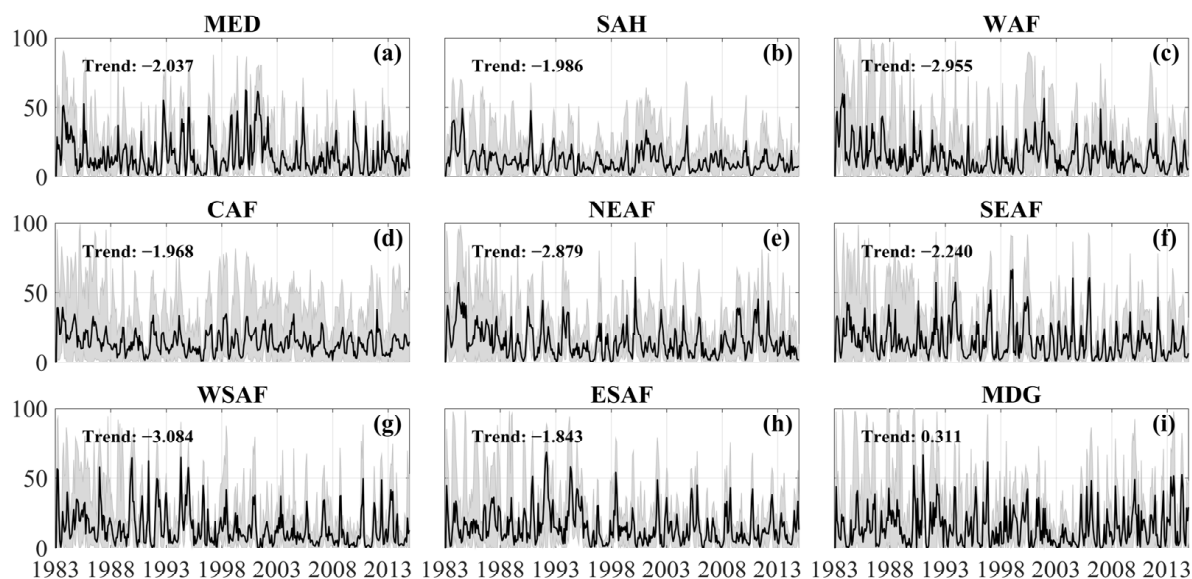


Figure 8. Percentage of Africa's subregions experiencing drought months. The black line is the mean of all the datasets and the grey shading shows the uncertainty range using maximum–minimum values from the individual datasets. Trend is the magnitude of linear change ($\% \text{ year}^{-1}$; scale: $\times 10^{-2}$) calculated using the Theil–Sen slope estimator. (a) MED; (b) SAH; (c) WAF; (d) CAF; (e) NEAF; (f) SEAF; (g) WSAF; (h) ESAF; and (i) MDG.

All regions regularly experience a 50% impact area but with a decreasing trend, ranging from -1.843% (ESAF) to -3.084% (WSAF), except for MDG, which displays an increasing trend of 0.311% . The impact of drought is less severe in the SAH and CAF regions, while more impact is noted for the MDG, MED, and WAF regions. Specifically, WSAF experiences a high impact from 1988 to 1995, which reduces from 2003 to 2008. On the other hand, NEAF experiences a high impact of above 50% during 1999, compared to other years during the study period. These findings indicate that the impact of drought events varies extensively across the different regions of Africa.

Figure 9 shows the interannual variability of drought impact areas for moderate drought months. The analysis reveals a high degree of variability, with MDG and CAF presenting the largest and smallest variability of 6.64 and 3.54%, respectively. The maximum drought impact area ranges from 19.91 (CAF) to 30.99% (ESAF), while the minimum drought impact area ranges from 0.00 (MDG) to 0.87% (CAF). This means that apart from MDG, all other regions have at least one pixel that experiences moderate drought during all months of the study period. The mean impact area ranges from 7.42 (SAH) to 9.21% (MED). The maximum drought impact area for severe drought is smaller than that for moderate drought.

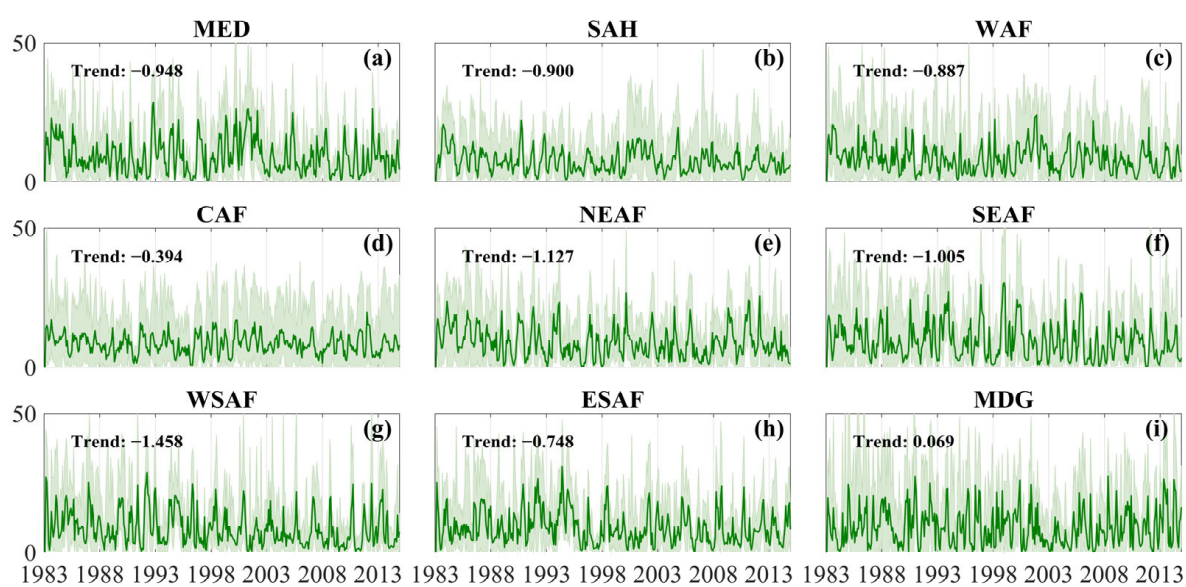


Figure 9. Percentage of Africa's subregions experiencing moderate drought conditions. The green line is the mean of all the datasets and the shading shows the uncertainty range using maximum–minimum values from the individual datasets. Trend is the magnitude of linear change ($\% \text{ year}^{-1}$; scale: $\times 10^{-2}$) calculated using the Theil–Sen slope estimator. (a) MED; (b) SAH; (c) WAF; (d) CAF; (e) NEAF; (f) SEAF; (g) WSAF; (h) ESAF; and (i) MDG.

The trends indicate that all regions show a decreasing drought impact area except for MDG (0.069%). CAF displays the smallest decreasing trend (-0.394%), while WSAF displays the largest (-1.458% %).

MED experiences several occurrences of drought impact areas larger than 20%, notably in 1992, 1996, 1999, and 2001. Interestingly SAH only experiences 2 months that barely reach 20%. WAF shows a drought impact area of more than 20% in late 2001. CAF does not experience drought impact areas of more than 20%. NEAF shows a drought impact area greater than 20% in 1984, 1994, and 2011. SEAF experiences a drought impact area of more than 20% in 1993, 1996/1997, 1998, 2000, and 2005/2006. WSAF shows a drought impact area greater than 20% in 1983, 1992, 1993, 1994, and 2000/2001. ESAF displays a drought impact area greater than 20% in 1992, 1994, and 1998. MDG experiences a drought impact area greater than 20% in 1985, 1991, 1993, 1995, 1996, 2000, 2013, and 2014.

Figure 10 shows the interannual variability of drought impact areas for severe drought months. The variability ranges from 2.47 (SAH) to 4.46% (MED) and the mean ranges from 2.81 (SAH) to 4.16% (MED). CAF and WSAF present the smallest and largest maximum drought impact area of 11.29% and 26.07%, respectively. Apart from SAH, WAF, CAF, and WSAF that have minimum drought impact areas of 0.10, 0.02, 0.10, and 0.04%, respectively; all other regions have minimum drought impact areas of 0.00%.

The trends for severe drought conditions also show an increasing drought area for MDG (0.188%). ESAF and WSAF show the smallest (-0.605%) and largest (-0.957%) decreasing trend, respectively.

Severe drought conditions are recurrent in all regions of Africa. Each year, at least one pixel in each region experiences severe drought, highlighting the severity and persistence of the problem across the continent.

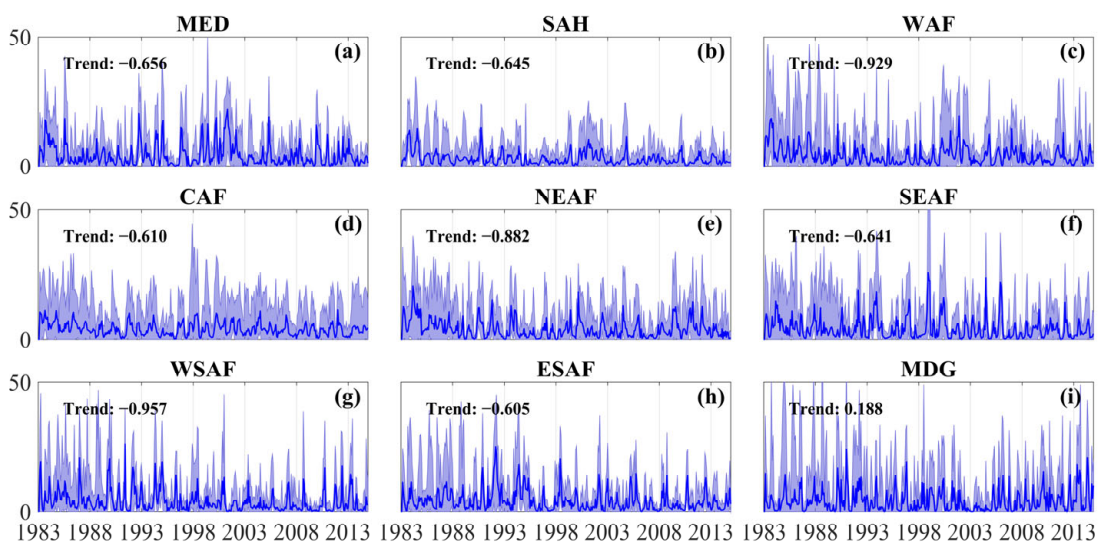


Figure 10. Percentage of Africa's subregions experiencing severe drought conditions. The blue line is the mean of all the datasets and the shading shows the uncertainty range using maximum–minimum values from the individual datasets. Trend is the magnitude of linear change ($\% \text{ year}^{-1}$; scale: $\times 10^{-2}$) calculated using the Theil–Sen slope estimator. (a) MED; (b) SAH; (c) WAF; (d) CAF; (e) NEAF; (f) SEAF; (g) WSAF; (h) ESAF; and (i) MDG.

Figure 11 shows the interannual variability of drought impact areas for extreme drought months. The mean and variability of drought impact areas range from 1.00 (SAH) to 2.36% (CAF) and 1.68 (SAH) to 3.39% (WAF), respectively. MED presents the largest maximum drought impact area (30.41%), while CAF shows the smallest maximum drought impact area (15.11%). All regions have a minimum drought impact area of 0.00%, except for CAF (0.01%). The maximum drought impact area for extreme drought is generally larger than that for severe drought.

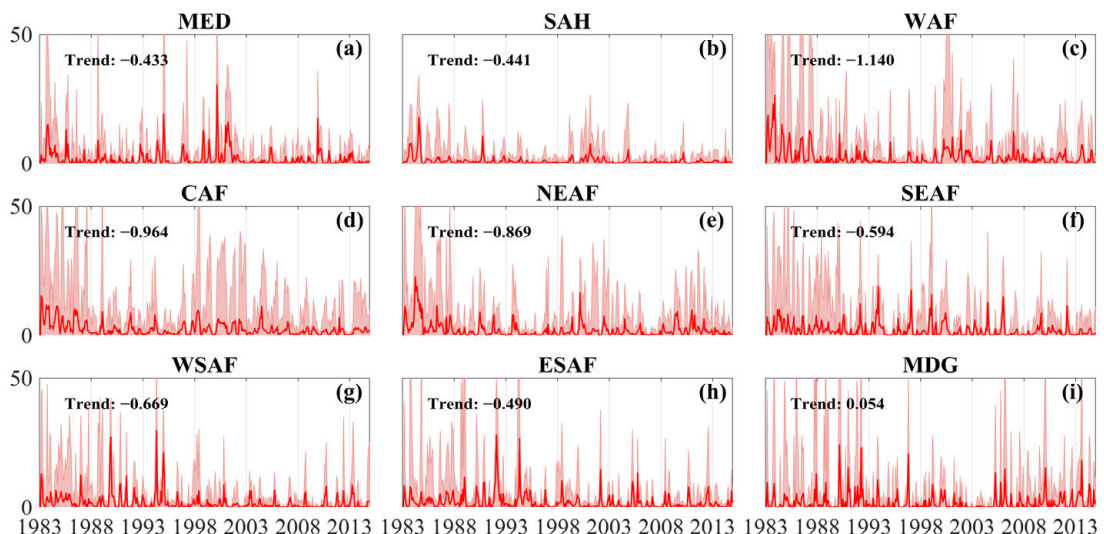


Figure 11. Percentage of Africa's subregions experiencing extreme drought conditions. The red line is the mean of all the datasets and the shading shows the uncertainty range using maximum–minimum values from the individual datasets. Trend is the magnitude of linear change ($\% \text{ year}^{-1}$; scale: $\times 10^{-2}$) calculated using the Theil–Sen slope estimator. (a) MED; (b) SAH; (c) WAF; (d) CAF; (e) NEAF; (f) SEAF; (g) WSAF; (h) ESAF; and (i) MDG.

MDG also shows an increasing drought impact area trend (0.054%) for extreme drought, while MED and WAF show the smallest (-0.433%) and largest (-1.140%) decreasing trend, respectively.

The impact area for extreme drought conditions is relatively low (with an average of 1.90%) compared to moderate and severe drought conditions. MED experiences extreme drought around the 2000s, and WSAF experiences extreme drought around 1989 and 1995.

The average drought impact area is largest for moderate drought, followed by severe and extreme drought conditions. Moderate drought also displays the largest variability, while extreme drought presents the smallest variability. Considering the maximum drought impact area, we note that severe drought has the smallest maximum drought-impact area. Moderate and extreme droughts have the largest impact over different regions (MED, WAF, and WSAF for extreme drought months).

Moderate droughts have an overall larger drought impact area decreasing trend, followed by severe and extreme droughts. WSAF displays the largest decreasing trend for moderate and severe drought, while WAF shows the largest decreasing trend for extreme drought. Although a linear trend calculated during the whole study period might not accurately portray the actual trend (since the trend might not be linear), the results provide information about the magnitude of the linear change during the study period.

4. Discussion

Our results indicate larger SPI-3 values over CAF and NEAF than across Eastern SAH and WSAF, which are consistent with recent literature. For instance, the global disaster alert and coordination system (GDACS) reported a drought that started in mid-January 2021 and lasted for a total of seven (7) months in the CAF region [70]. Furthermore, across parts of SEAF and ESAF, the drought, which started by the end of March 2022, lasted twelve (12) months [71].

Generally, our results based on a 3-month time scale align with the need for monitoring soil-moisture changes over time and are critical for deciding when to plant crops, especially in a rainfed cropping system [72]. Only 5% of the cultivated area in sub-Saharan Africa is irrigated [73], while CAF, SAH, WSAF, and other sub-Saharan African regions depend on a rainfed cropping system [74,75]. The SPI-3-based results indicate the susceptibility of such regions to a reduction in crop yields. On average, yields of crops from rainfed areas are 2.7 times less than those from irrigated areas [76]. Due to climate variability, precipitation is progressively becoming unpredictable with increasing frequency of drought events, thereby compounding the vulnerability of smallholder farmers to low crop yields. One option for farmers in drought-prone areas is to adopt irrigation. However, irrigation entails equipment and accessories installation, and operation and maintenance costs. Unfortunately, most farmers cannot afford these costs, which explains why irrigation is limited across sub-Saharan Africa [77]. Farmers can also adopt drought-resistant crops in regions such as CAF, SAH, and WSAF. Furthermore, given the uncertainty in yield-gap closure, another option would be for the government in drought-prone areas to promote nonfarm income-generating activities for the local citizens [74,78].

One limitation of the approach used in this study is that the standardisation of precipitation to derive SPI lacks the capability of distinguishing regions that can be more drought-prone than others [79]. Ideally, two equal SPI values from different regions cannot be taken to mean a similar precipitation deficit [79]. Furthermore, regional differences in precipitation variability mean that some regions have lower long-term mean precipitation totals than other areas. In fact, spatial variation in the long-term precipitation mean can show the various types of climates, thereby indicating differences in susceptibility to droughts. Areas with low precipitation can be characterised by a low standard deviation (indicating low precipitation variability; see Figure A2), leading to large SPI values. On the other hand, areas with large precipitation totals and high intermittency tend to be characterised by a large precipitation standard deviation (indicating high variability) and these lead to small SPI values. The influence of precipitation variability on SPIs is more pronounced with low (e.g., 1-, 2-, and 3-month) time scales [79]. Therefore, caution should

be taken when interpreting the SPI values. Furthermore, readers should be careful when interpreting results over regions such as SAH, since these regions have a lack of data and thus very limited evidence [1].

5. Conclusions

Africa is strongly affected by precipitation variability and its extremes. This study employs the SPI technique to analyse the spatiotemporal variability of different drought levels over Africa and its nine climate subregions from an ensemble of multisource datasets (gauge-based, satellite-based and reanalysis). The present study does not attempt to explain the mechanism for drought formation but instead analyses various drought characteristics (duration, events, frequency, intensity, and severity) for all drought months and moderate, severe, and extreme drought conditions across Africa.

The study demonstrates that drought events occur across the continent, with equatorial regions experiencing smaller SPI values for all drought months, while Eastern SAH and WSAF have larger SPI values for moderate drought months. Eastern SAH and WSAF regions show higher SPI values for severe and extreme drought months, while the rest of the continent has evenly distributed small SPI values. The interannual variability of drought levels shows that drought variability differs across all regions, with extreme drought months having the largest interannual variability, followed by all and severe drought months. The trend analysis of SPI shows significantly increasing drought trends in most regions of Africa, especially in WAF, CAF, SEAF, and ESAF. Drought duration varies greatly across different regions of Africa, with some areas experiencing longer and more severe droughts than others. The equatorial regions of Africa experience more frequent and severe drought events than other regions, with longer durations and smaller SPI values.

MDG experiences the lowest impact of drought for moderate and severe drought categories (and second lowest for all and extreme drought months). On the other hand, SAH is strongly impacted by moderate and severe drought conditions while experiencing the lowest extreme drought months compared to other regions, suggesting that severe and extreme droughts are less frequent but more severe in this region. Meanwhile, CAF receives the highest drought impact for extreme drought conditions, followed by NEAF and WAF. The CAF region experiences a low number of drought events but with long duration for all and extreme drought months. Overall, we note that the findings from all drought months do not accurately portray the situation observed for different drought levels.

This work highlights the importance of analysing drought at different drought levels to accurately portray the extent of drought impact. The findings have implications for the planning and managing of droughts and the adaptation strategies needed to enhance community resilience to changing drought situations, particularly in regions with high population density and agricultural activities. These strategies should prioritise the early detection and prediction of drought events and the development of adaptive measures to minimise the impact of drought on vulnerable communities and ecosystems. In addition, it is important to continue monitoring drought-prone regions to better understand the factors contributing to drought variability and to develop effective strategies to reduce the impacts of drought on communities and the environment.

Author Contributions: Conceptualization: K.T.C.L.K.S., B.O.A., C.O. and V.O.; methodology: K.T.C.L.K.S., B.O.A., C.O. and V.O.; visualization: K.T.C.L.K.S.; validation: X.Z., C.O. and V.O.; formal analysis: K.T.C.L.K.S., B.O.A. and Z.W.S.; data curation: K.T.C.L.K.S.; writing—original draft preparation: K.T.C.L.K.S., B.O.A. and V.O.; writing—review and editing: X.Z., C.O. and Z.W.S. All authors have read and agreed to the published version of the manuscript.

Funding: This research is funded by project number 560120054. This research was supported by the Brain Pool program funded by the Ministry of Science and ICT through the National Research Foundation of Korea (NRF-2022H1D3A2A02063155).

Data Availability Statement: FROGS: <https://doi.org/10.14768/06337394-73A9-407C-9997-0E380DAC5598> (accessed on 6 September 2022). NCL: <https://www.ncl.ucar.edu/>. SPI-NCL: https://www.ncl.ucar.edu/Document/Functions/Built-in/dim_spi_n.shtml.

Acknowledgments: The authors thank the developers of the FROGS database for making their data openly available.

Conflicts of Interest: The authors declare no conflict of interest.

Appendix A

Appendix A.1. Study Area

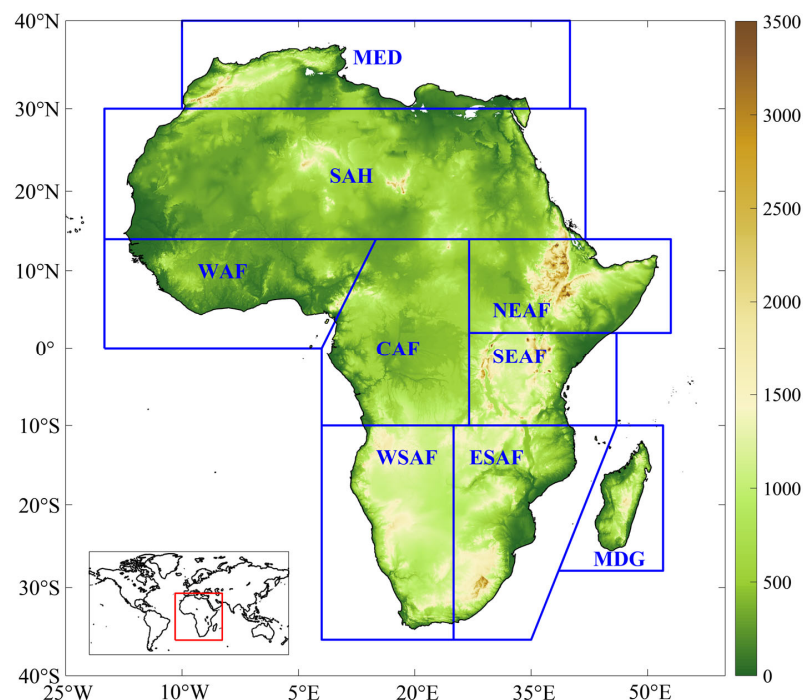


Figure A1. Map of Africa and its 9 subregions (delineated by blue boxes). The background colour shows the terrain elevation (m) and the inset shows the geographical position of the African continent (red box). MED: Mediterranean; SAH: Sahara; WAF: Western Africa; CAF: Central Africa; NEAF: Northern Eastern Africa; SEAF: Southern Eastern Africa; WSAF: Western Southern Africa; ESAF: Eastern Southern Africa; and MDG: Madagascar.

Appendix A.2. Precipitation Climatology

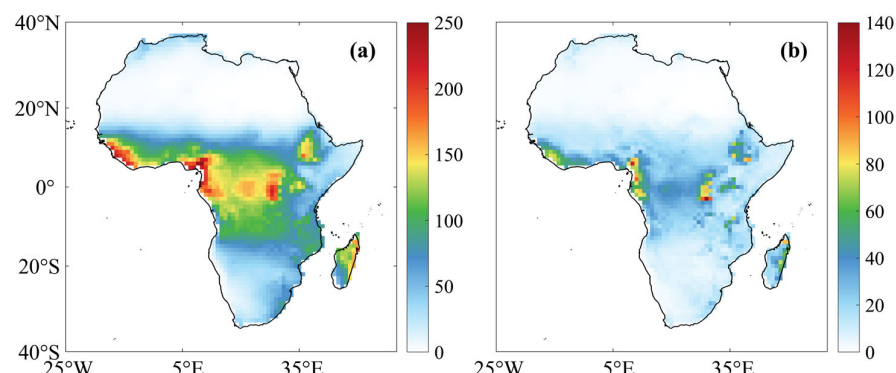


Figure A2. Spatial distribution of monthly-accumulated precipitation (mm) over Africa during 1983–2014 from gauge-based, satellite-based, and reanalysis data. (a) Precipitation mean; and (b) precipitation standard deviation.

References

- IPCC. Summary for Policymakers. In *Climate Change 2021: The Physical Science Basis. Contribution of Working Group I to the Sixth Assessment Report of the Intergovernmental Panel on Climate Change*; Masson-Delmotte, V., Zhai, P., Pirani, A., Connors, S.L., Péan, C., Berger, S., Caud, N., Chen, Y., Goldfarb, L., Gomis, M.I., et al., Eds.; Cambridge University Press: Cambridge, UK; New York, NY, USA, 2021; pp. 3–32.
- WMO. *State of the Climate in Africa 2021*; WMO: Geneva, Switzerland, 2022.
- Abrams, L. *Unlocking the Potential of Enhanced Rainfed Agriculture*; Report no. 39; Stockholm International Water Institute: Stockholm, Sweden, 2018.
- Lim Kam Sian, K.T.C.; Wang, J.; Ayugi, B.O.; Nooni, I.K.; Ongoma, V. Multi-Decadal Variability and Future Changes in Precipitation over Southern Africa. *Atmosphere* **2021**, *12*, 742. [[CrossRef](#)]
- Kedir, A.M. Environment and Climate Change in Africa in An Era of Sustainable Development Goals. In *From Millennium Development Goals to Sustainable Development Goals: Rethinking African Development*; Hanson, K.T., Puplampu, K.P., Shaw, T.M., Eds.; Routledge: London, UK, 2017; p. 15.
- Dinku, T.; Faniriantsoa, R.; Islam, S.; Nsengiyumva, G.; Grossi, A. The Climate Data Tool: Enhancing Climate Services Across Africa. *Front. Clim.* **2022**, *3*, 787519. [[CrossRef](#)]
- Bessenbacher, V.; Seneviratne, S.I.; Gudmundsson, L. CLIMFILL v0. 9: A framework for intelligently gap filling Earth observations. *Geosci. Model Dev.* **2022**, *15*, 4569–4596. [[CrossRef](#)]
- Cornes, R.C.; van der Schrier, G.; van den Besselaar, E.J.M.; Jones, P.D. An Ensemble Version of the E-OBS Temperature and Precipitation Data Sets. *J. Geophys. Res. Atmos.* **2018**, *123*, 9391–9409. [[CrossRef](#)]
- Dosio, A.; Pinto, I.; Lennard, C.; Sylla, M.B.; Jack, C.; Nikulin, G. What Can We Know About Recent Past Precipitation Over Africa? Daily Characteristics of African Precipitation from a Large Ensemble of Observational Products for Model Evaluation. *Earth Sp. Sci.* **2021**, *8*, e2020EA001466. [[CrossRef](#)]
- Haile, G.G.; Tang, Q.; Sun, S.; Huang, Z.; Zhang, X.; Liu, X. Droughts in East Africa: Causes, impacts and resilience. *Earth-Science Rev.* **2019**, *193*, 146–161. [[CrossRef](#)]
- WFP. *Horn of Africa: Extreme Drought Deepens Hunger in a Region Facing Conflict*; WFP: Rome, Italy, 2022.
- Ongoma, V.; Chen, H. Temporal and spatial variability of temperature and precipitation over East Africa from 1951 to 2010. *Meteorol. Atmos. Phys.* **2017**, *129*, 131–144. [[CrossRef](#)]
- Omondi, O.A.; Lin, Z. Trend and spatial-temporal variation of drought characteristics over equatorial East Africa during the last 120 years. *Front. Earth Sci.* **2023**, *10*, 1064940. [[CrossRef](#)]
- Gebrechorkos, S.H.; Hülsmann, S.; Bernhofer, C. Analysis of climate variability and droughts in East Africa using high-resolution climate data products. *Glob. Planet. Change* **2020**, *186*, 103130. [[CrossRef](#)]
- Masih, I.; Maskey, S.; Mussá, F.E.F.; Trambauer, P. A review of droughts on the African continent: A geospatial and long-term perspective. *Hydrol. Earth Syst. Sci.* **2014**, *18*, 3635–3649. [[CrossRef](#)]
- Haile, G.G.; Tang, Q.; Li, W.; Liu, X.; Zhang, X. Drought: Progress in broadening its understanding. *WIREs Water* **2019**, *7*, e1407. [[CrossRef](#)]
- Rodríguez-Fonseca, B.; Mohino, E.; Mechoso, C.R.; Caminade, C.; Biasutti, M.; Gaetani, M.; Garcia-Serrano, J.; Vizy, E.K.; Cook, K.; Xue, Y.; et al. Variability and Predictability of West African Droughts: A Review on the Role of Sea Surface Temperature Anomalies. *J. Clim.* **2015**, *28*, 4034–4060. [[CrossRef](#)]
- Doukoro, D.; Abbey, G.A.; Kalifa, T. Drought Monitoring and Assessment of Climate Parameters Variability in Koutiala and San Districts, Mali. *Am. J. Clim. Chang.* **2022**, *11*, 230–249. [[CrossRef](#)]
- Addi, M.; Asare, K.; Fosuhene, S.K.; Ansah-narh, T.; Aidoo, K.; Botchway, C.G. Impact of Large-Scale Climate Indices on Meteorological Drought of Coastal Ghana. *Adv. Meteorol.* **2021**, *2021*, 8899645. [[CrossRef](#)]
- Belhassan, K. *Managing Drought and Water Stress in Northern Africa*; IntechOpen: London, UK, 2022.
- Nxumalo, G.; Bashir, B.; Alsafadi, K.; Bachir, H.; Harsányi, E.; Arshad, S.; Mohammed, S. Meteorological Drought Variability and Its Impact on Wheat Yields across South Africa. *Int. J. Environ. Res. Public Health* **2022**, *19*, 16469. [[CrossRef](#)] [[PubMed](#)]
- Pascale, S.; Kapnick, S.B.; Delworth, T.L.; Cooke, W.F. Increasing risk of another Cape Town “Day Zero” drought in the 21st century. *Proc. Natl. Acad. Sci. USA* **2020**, *117*, 29495–29503. [[CrossRef](#)] [[PubMed](#)]
- Nicholson, S.E. An Analysis of the ENSO Signal in the Tropical Atlantic and Western Indian Oceans. *Int. J. Climatol.* **1997**, *17*, 345–375. [[CrossRef](#)]
- Moura, M.N.; Aimola, L.L. The Role of Sea Surface Temperature in the Rainfall Regime in Sub-Saharan Africa. *Rev. Bras. Climatol.* **2019**, *25*, 1–14. [[CrossRef](#)]
- Iturbide, M.; Gutiérrez, J.M.; Alves, L.M.; Bedia, J.; Cerezo-Mota, R.; Cimadevilla, E.; Cofiño, A.S.; Di Luca, A.; Faria, S.H.; Gorodetskaya, I.; et al. An update of IPCC climate reference regions for subcontinental analysis of climate model data: Definition and aggregated datasets. *Earth Syst. Sci. Data* **2020**, *12*, 2959–2970. [[CrossRef](#)]
- Nicholson, S.E. The ITCZ and the seasonal cycle over equatorial Africa. *Bull. Am. Meteorol. Soc.* **2018**, *99*, 337–348. [[CrossRef](#)]
- Thoithi, W.; Blamey, R.C.; Reason, C.J.C. Dry Spells, Wet Days, and Their Trends Across Southern Africa During the Summer Rainy Season. *Geophys. Res. Lett.* **2021**, *48*, e2020GL091041. [[CrossRef](#)]
- Lim Kam Sian, K.T.C.; Dosio, A.; Ayugi, B.O.; Hagan, D.F.T.; Kebacho, L.L.; Ongoma, V. Dominant modes of precipitation over Africa, and their associated atmospheric circulations from observations. *Int. J. Climatol.* **2023**. [[CrossRef](#)]

29. Roca, R.; Alexander, L.V.; Potter, G.; Bador, M.; Jucá, R.; Contractor, S.; Bosilovich, M.G.; Cloché, S. FROGS: A daily $1^\circ \times 1^\circ$ gridded precipitation database of rain gauge, satellite and reanalysis products. *Earth Syst. Sci. Data* **2019**, *11*, 1017–1035. [[CrossRef](#)]
30. Onyutha, C. Trends and variability in African long-term precipitation. *Stoch. Environ. Res. Risk Assess.* **2018**, *32*, 2721–2739. [[CrossRef](#)]
31. Washington, R.; James, R.; Pearce, H.; Pokam, W.M.; Moufouma-okia, W. Congo Basin rainfall climatology: Can we believe the climate models? *Philos. Trans. R. Soc. B* **2013**, *368*, 20120296. [[CrossRef](#)]
32. Maidment, R.I.; Allan, R.P.; Black, E. Recent observed and simulated changes in precipitation over Africa. *Geophys. Res. Lett.* **2015**, *42*, 8155–8164. [[CrossRef](#)]
33. Onyutha, C.; Tabari, H.; Taye, M.T.; Nyandwaro, G.N.; Willems, P. Analyses of rainfall trends in the Nile River Basin. *J. Hydro-Environ. Res.* **2016**, *13*, 36–51. [[CrossRef](#)]
34. Onyutha, C. Analyses of rainfall extremes in East Africa based on observations from rain gauges and climate change simulations by CORDEX RCMs. *Clim. Dyn.* **2020**, *54*, 4841–4864. [[CrossRef](#)]
35. Kidd, C.; Huffman, G. Global precipitation measurement. *Meteorol. Appl.* **2011**, *18*, 334–353. [[CrossRef](#)]
36. Kidd, C.; Levizzani, V. Status of satellite precipitation retrievals. *Hydrol. Earth Syst. Sci.* **2011**, *15*, 1109–1116. [[CrossRef](#)]
37. Bosilovich, M.G.; Chen, J.; Robertson, F.R.; Adler, R.F. Evaluation of Global Precipitation in Reanalyses. *J. Appl. Meteorol. Climatol.* **2008**, *47*, 2279–2299. [[CrossRef](#)]
38. Fujiwara, M.; Wright, J.S.; Manney, G.L.; Gray, L.J.; Anstey, J.; Birner, T.; Davis, S.; Gerber, E.P.; Harvey, V.L.; Hegglin, M.I.; et al. Introduction to the SPARC Reanalysis Intercomparison Project (S-RIP) and overview of the reanalysis systems. *Atmos. Chem. Phys.* **2017**, *17*, 1417–1452. [[CrossRef](#)]
39. Xie, P.-P.; Chen, M.; Shi, W. CPC unified gauge-based analysis of global daily precipitation. In Proceedings of the 24th Conference on Hydrology, The 90th American Meteorological Society Annual Meeting, Atlanta, GA, USA, 16–21 January 2010.
40. Ziese, M.; Rauthe-Schöch, A.; Becker, A.; Finger, P.; Meyer-Christoffer, A.; Schneider, U. GPCC Full Data Daily Version 2018 at 1.0° : Daily Land-Surface Precipitation from Rain-Gauges Built on GTS-Based and Historic Data; Global Precipitation Climatology Centre: Offenbach, Germany, 2018.
41. Ziese, M.; Rauthe-Schöch, A.; Becker, A.; Finger, P.; Rustemeier, E.; Schneider, U. GPCC Full Data Daily Version 2020 at 1.0° : Daily Land-Surface Precipitation from Rain-Gauges Built on GTS-Based and Historic Data; Global Precipitation Climatology Centre: Offenbach, Germany, 2020.
42. Contractor, S.; Donat, M.G.; Alexander, L.V.; Ziese, M.; Meyer-christoffer, A.; Schneider, U.; Rustemeier, E.; Becker, A.; Durre, I.; Vose, R.S. Rainfall Estimates on a Gridded Network (REGEN)—A global land-based gridded dataset of daily precipitation from 1950 to 2016. *Hydrol. Earth Syst. Sci.* **2020**, *24*, 919–943. [[CrossRef](#)]
43. Novella, N.S.; Thiaw, W.M. African Rainfall Climatology Version 2 for Famine Early Warning Systems. *J. Appl. Meteorol. Climatol.* **2013**, *52*, 588–606. [[CrossRef](#)]
44. Funk, C.; Peterson, P.; Landsfeld, M.; Pedreros, D.; Verdin, J.; Shukla, S.; Husak, G.; Rowland, J.; Harrison, L.; Hoell, A.; et al. The climate hazards infrared precipitation with stations—A new environmental record for monitoring extremes. *Sci. Data* **2015**, *2*, 150066. [[CrossRef](#)]
45. Sadeghi, M.; Nguyen, P.; Naeini, M.R.; Hsu, K.; Braithwaite, D.; Sorooshian, S. PERSIANN-CCS-CDR, a 3-hourly 0.04° global precipitation climate data record for heavy precipitation studies. *Sci. Data* **2021**, *8*, 157. [[CrossRef](#)]
46. Ashouri, H.; Hsu, K.; Sorooshian, S.; Braithwaite, D.; Knapp, K.R.; Cecil, L.D.; Nelson, B.R.; Prat, O.P. PERSIANN-CDR Daily Precipitation Climate Data Record from Multisatellite Observations for Hydrological and Climate Studies. *Bull. Am. Meteorol. Soc.* **2015**, *96*, 69–83. [[CrossRef](#)]
47. Maidment, R.I.; Grimes, D.; Black, E.; Tarnavsky, E.; Young, M.; Greatrex, H.; Allan, R.P.; Stein, T.; Nkonde, E.; Senkunda, S.; et al. A new, long-term daily satellite-based rainfall dataset for operational monitoring in Africa. *Sci. Data* **2017**, *4*, 170063. [[CrossRef](#)]
48. Saha, S.; Moorthi, S.; Pan, H.L.; Wu, X.; Wang, J.; Nadiga, S.; Tripp, P.; Kistler, R.; Woollen, J.; Behringer, D.; et al. The NCEP climate forecast system reanalysis. *Bull. Am. Meteorol. Soc.* **2010**, *91*, 1015–1057. [[CrossRef](#)]
49. Hersbach, H.; Bell, B.; Berrisford, P.; Hirahara, S.; Horányi, A.; Nicolas, J.; Peubey, C.; Radu, R.; Bonavita, M.; Dee, D.; et al. The ERA5 global reanalysis. *Q. J. R. Meteorol. Soc.* **2020**, *146*, 1999–2049. [[CrossRef](#)]
50. Dee, D.P.; Uppala, S.M.; Simmons, A.J.; Berrisford, P.; Poli, P.; Kobayashi, S.; Andrae, U.; Balmaseda, M.A.; Balsamo, G.; Bauer, P.; et al. The ERA-Interim reanalysis: Configuration and performance of the data assimilation system. *Q. J. R. Meteorol. Soc.* **2011**, *137*, 553–597. [[CrossRef](#)]
51. Dirmeyer, P.A.; Gao, X.; Zhao, M.; Guo, Z.; Oki, T.; Hanasaki, N. GSWP-2: Multimodel Analysis and Implications for Our Perception of the Land Surface. *Bull. Am. Meteorol. Soc.* **2006**, *87*, 1381–1398. [[CrossRef](#)]
52. Kobayashi, S.; Ota, Y.; Harada, Y.; Ebita, A.; Moriya, M.; Onoda, H.; Onogi, K.; Kamahori, H.; Kobayashi, C.; Endo, H.; et al. The JRA-55 Reanalysis: General Specifications and Basic Characteristics. *J. Meteorol. Soc. Japan* **2015**, *93*, 5–48. [[CrossRef](#)]
53. Rienecker, M.M.; Suarez, M.J.; Gelaro, R.; Todling, R.; Bacmeister, J.; Liu, E.; Bosilovich, M.G.; Schubert, S.D.; Takacs, L.; Kim, G.-K.; et al. MERRA: NASA’s Modern-Era Retrospective Analysis for Research and Applications. *J. Clim.* **2011**, *24*, 3624–3648. [[CrossRef](#)]
54. Gelaro, R.; McCarty, W.; Suárez, M.J.; Todling, R.; Molod, A.; Takacs, L.; Randles, C.A.; Darmenov, A.; Bosilovich, M.G.; Reichle, R.; et al. The Modern-Era Retrospective Analysis for Research and Applications, Version 2 (MERRA-2). *J. Clim.* **2017**, *30*, 5419–5454. [[CrossRef](#)]

55. McKee, T.B.; Doesken, N.J.; Kleist, J. The relationship of drought frequency and duration to time scales. In Proceedings of the Eight Conference on Applied Climatology, Anaheim, CA, USA, 17–22 January 1993; pp. 17–22.
56. McKee, T.B.; Doesken, N.J.; Kleist, J. Drought Monitoring with Multiple Time Scales. In Proceedings of the 9th Conference on Applied Climatology, Dallas, TX, USA, 15–20 January 1995; pp. 233–236.
57. Nicholson, S.E. Climate and climatic variability of rainfall over eastern Africa. *Rev. Geophys.* **2017**, *55*, 590–635. [CrossRef]
58. Guttman, N.B. Accepting the Standardized Precipitation Index: A Calculation Algorithm. *J. Am. Water Resour. Assoc.* **1999**, *35*, 311–322. [CrossRef]
59. Thom, H.C.S. *Some Methods of Climatological Analyses*; Secretariat of the World Meteorological Organization: Geneva, Switzerland, 1966.
60. Wilks, D.S. *Statistical Methods in the Atmospheric Science: An Introduction*; Academic Press: Cambridge, MA, USA, 1995.
61. Yevjevich, V. Objective Approach to Definitions and Investigations of Continental Hydrologic Droughts. Ph.D. Thesis, Colorado State University, Fort Collins, CO, USA, 1967.
62. Sen, P.K. Estimates of the Regression Coefficient Based on Kendall’s Tau. *J. Am. Stat. Assoc.* **1968**, *63*, 1379–1389. [CrossRef]
63. Mann, H.B. Nonparametric tests against trend. *J. Econom. Soc.* **1945**, *13*, 245–259. [CrossRef]
64. Kendall, M. *Rank Correlation Methods*, 4th ed.; Charles Griffin: San Francisco, CA, USA, 1975.
65. Ayugi, B.O.; Tan, G. Recent trends of surface air temperatures over Kenya from 1971 to 2010. *Meteorol. Atmos. Phys.* **2019**, *131*, 1401–1413. [CrossRef]
66. Karim, R.; Tan, G.; Ayugi, B.; Babaousmail, H.; Liu, F. Evaluation of historical CMIP6 model simulations of seasonal mean temperature over Pakistan during 1970–2014. *Atmosphere* **2020**, *11*, 1005. [CrossRef]
67. Ngoma, H.; Wang, W.; Ojara, M.; Ayugi, B. Assessing current and future spatiotemporal precipitation variability and trends over Uganda, East Africa, based on CHIRPS and regional climate model datasets. *Meteorol. Atmos. Phys.* **2021**, *133*, 823–843. [CrossRef]
68. Lim Kam Sian, K.T.C.; Hagan, D.F.T.; Ayugi, B.O.; Nooni, I.K.; Ullah, W.; Babaousmail, H.; Ongoma, V. Projections of precipitation extremes based on bias-corrected Coupled Model Intercomparison Project phase 6 models ensemble over southern Africa. *Int. J. Climatol.* **2022**, *42*, 8269–8289. [CrossRef]
69. Babaousmail, H.; Ayugi, B.O.; Ojara, M.; Ngoma, H.; Oduro, C.; Mumo, R.; Ongoma, V. Projection of the diurnal temperature range over Africa based on CMIP6 simulations. *J. Afr. Earth Sci.* **2023**, *200*, 104883. [CrossRef]
70. GDACS Overall Green Alert Drought for D.R. Congo. 2021. Available online: <https://www.gdacs.org/report.aspx?eventid=1014756&episodeid=6&eventtype=DR> (accessed on 21 April 2023).
71. GDACS Overall Orange Alert Drought for East Africa. 2022. Available online: <https://www.gdacs.org/report.aspx?eventid=1014742&episodeid=69&eventtype=DR> (accessed on 21 April 2023).
72. Ocen, E.; de Bie Kees, C.A.J.M.; Onyutha, C. Investigating false start of the main growing season: A case of Uganda in East Africa. *Heliyon* **2021**, *7*, e08428. [CrossRef]
73. You, L.Z. *Africa: Irrigation Investment Needs in Sub-Saharan Africa, Africa Infrastructure Country Diagnostic Background Paper*; No. 9; World Bank: Washington DC, USA, 2008.
74. Onyutha, C. African crop production trends are insufficient to guarantee food security in the sub-Saharan region by 2050 owing to persistent poverty. *Food Secur.* **2018**, *10*, 1203–1219. [CrossRef]
75. World Bank. *Southern Africa Drought Resilience Initiative (SADRI): DRC Drought Profile*; World Bank: Washington, DC, USA, 2021.
76. United Nations. *Managing Water under Uncertainty and Risk. World Water Development*; Report 4; United Nations: New York, NY, USA, 2012.
77. Onyutha, C. African food insecurity in a changing climate: The roles of science and policy. *Food Energy Secur.* **2019**, *8*, e00160. [CrossRef]
78. Kristjanson, P.; Mango, N.; Krishna, A.; Radeny, M.; Johnson, N. Understanding poverty dynamics in Kenya. *J. Int. Dev.* **2010**, *22*, 978–996. [CrossRef]
79. Angelidis, P.; Maris, F.; Kotsovios, N.; Hrissanthou, V. Computation of Drought Index SPI with Alternative Distribution Functions. *Water Resour. Manag.* **2012**, *26*, 2453–2473. [CrossRef]

Disclaimer/Publisher’s Note: The statements, opinions and data contained in all publications are solely those of the individual author(s) and contributor(s) and not of MDPI and/or the editor(s). MDPI and/or the editor(s) disclaim responsibility for any injury to people or property resulting from any ideas, methods, instructions or products referred to in the content.